Modification of n-type Silicon Electrodes with Nano-Meter Sized Platinum Particles for Efficient Photoelectrochemical Solar Cells

by

Shinji YAE

Department of Chemistry
Graduate School of Engineering Science
Osaka University

1997

Contents

General Introduction

Since the oil crisis in 1973, the solar energy has attracted strong attention as an inexhaustible new energy source for the present and future human society. In addition, the global environmental problems have arisen recently, such as the green house effect due to carbon dioxide increase in the atmosphere and the acid rains, and are getting more and more serious. The clean solar energy is thus attracting more and more attention these days.

For the utilization of the solar energy, the photovoltaic conversion using solar cells is the most promising method. So far, main studies have been made on the p-n junction solar cells. In particular, many studies have been made on high-efficiency single-crystal silicon (Si) solar cells. Green et al. reported 24 % of the conversion efficiency for the PERL (passivated emitter and rear locally diffused) cells under the global AM1.5 spectrum (1000 Wm^{-2}) [1-3]. Although this efficiency is the highest for the Si solar cells and approaching the theoretical limit, the PERL cell has very elaborate structure, leading to too high production cost for large-scale practical uses. The low energy density of 700 to 1000 Wm^{-2} of the solar light requires the realization of not only high efficiency but also low-cost solar cells.

For the development of high-efficiency and low-cost solar cells, many kinds of semiconductors, such as polycrystalline (or multicrystalline) Si wafers, amorphous Si thin films, polycrystalline Si thin films, cadmium telluride (CdTe), and copper indium selenide ($CuInSe_2$), have been studied as the promising low cost materials [2-8]. For the compound semiconductors like CdTe and $CuInSe_2$, the elements Cd and In are not enough in amount as the resources on the earth. The production cost of the polycrystalline Si wafers is still high. The amorphous Si thin films have problems of no enough high efficiency nor long term stability. Thus, the

polycrystalline Si thin films are, at present, expected to be the most promising material for the high-efficiency and low-cost solar cells. In order to utilize effectively such raw granular materials, the p-n junction method is not necessarily suitable for getting a high efficiency. It is thus very important to find a suitable method to get a good junction for such raw granular materials.

Photoelectrochemical (PEC) solar cells are a promising candidate for such purpose [9, 10], because they can be fabricated simply by immersing a semiconductor electrode and a counterelectrode into a redox electrolyte solution [11]. The PEC solar cells have another advantage that they can directly convert the solar energy into storable chemical energy, through reactions such as water splitting into hydrogen and oxygen [10, 12-14], the production of hydrogen and iodine from hydrogen iodide [15], and the reduction of carbon dioxide to hydrocarbons [16] or carbon monoxide [17, 18]. Unfortunately, the PEC solar cells at present have a problem that they have no sufficient long-term stability.

In the laboratory to which the author belongs, both PEC and solid-state solar cells of a new type have been developed, in which a Si wafer is modified with ultrafine metal particles [19, 20]. Figure 1 shows schematic cross-sections of the solar cells. The PEC solar cells using a single-crystal n-type Si (n-Si) electrode modified with ultrafine platinum (Pt) particles generate open-circuit photovoltages (V_{OC}'s) of 0.62 to 0.68 V, considerably higher than those (ca. 0.59 V) of the conventional p-n junction Si solid-state solar cells with similar simple structure. The PEC solar cells are enough stable for laboratory experiments but not enough for practical application. The solid-state solar cells (Fig. 1B) operate by the same principle as for the PEC cells, but, at present, give only a V_{OC} of 0.59 V at highest and a conversion efficiency of 10.4 % due to the formation of surface defects

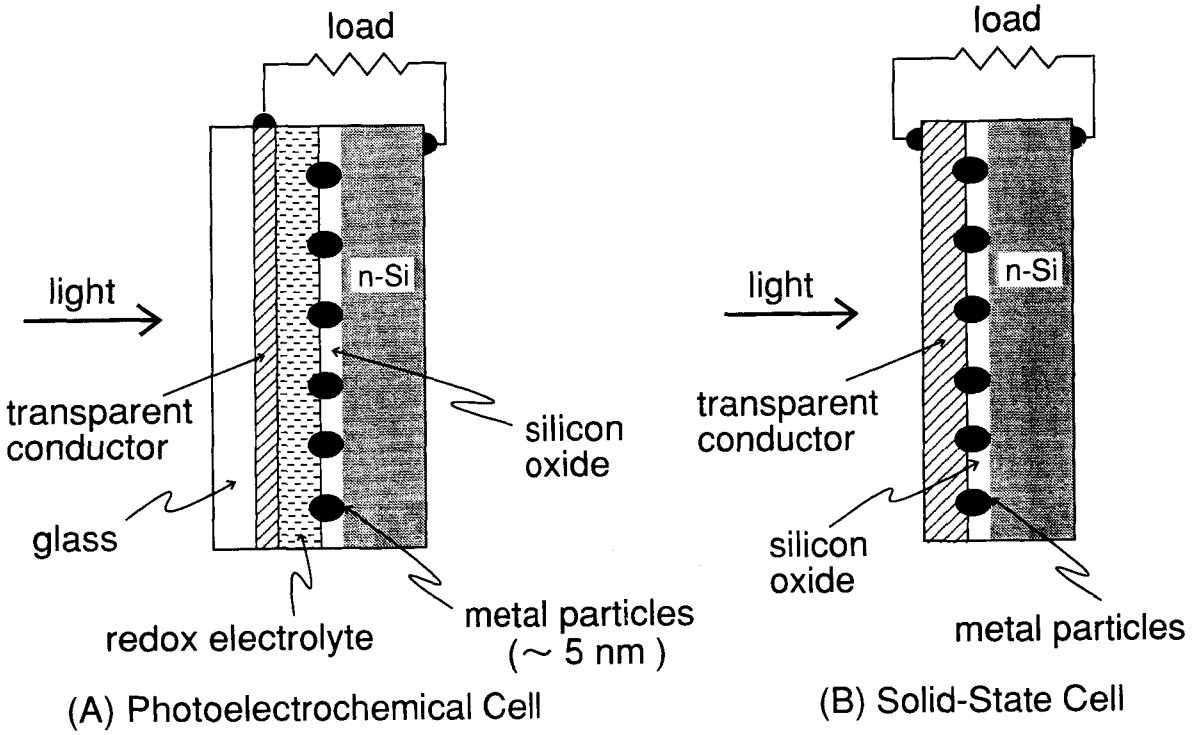

Figure 1. Schematic cross-sections of a photoelectrochemical (PEC) solar cell (A) and a solid-state solar cell (B), equipped with an n-Si wafer modified with ultrafine metal particles.

(surface states) during the deposition of transparent conductor (TC) on the Pt-modified n-Si wafer [21]. This problem will be solved in the near future by intervening a thin (ca. 3 nm) organic layer between Si and TC [21]. The solid-state solar cells are much more stable than the PEC cells, and expected to be enough stable for practical use. The fabrication method of these solar cells (Fig. 1) can be applied to polycrystalline Si thin films [22]. No high-temperature treatment nor lithographic technique are necessary for making solar cells of this type. Thus, this type of solar cells is expected to open a new approach to high-efficiency and low-cost solar cells.

The operation principle of this type of solar cells is explained as follows [19, 20]. Photogenerated holes in n-Si transfer to the redox solution (or transparent conductor) through the Pt particles, thus leading to a steady photocurrent. With no Pt, the photocurrent decays rapidly for the PEC cells (Fig. 1A) or gradually for the solid-state cells (Fig. 1B). The surface band energies of n-Si are modulated by the deposition of Pt particles. However, the effective barrier height is nearly the same as that for no Pt in case where the size of the Pt particles (or more correctly, the size of the areas of direct Pt-Si contacts) is small enough, much smaller than the width of the space charge layer. Thus, a very high barrier height, nearly equal to the band-gap, can be obtained if one uses a redox couple with an enough high redox potential for the PEC cells (Fig. 1A) or a transparent conductor with an enough large work function for the solid-state cells (Fig. 1B). Also, a major part of the n-Si surface is covered with a thin Si-oxide layer and passivated, and hence the electron-hole recombination rate at the n-Si surface is maintained quite low. For these reasons, very high V_{OC} can be generated.

For obtaining high efficiencies and reproducible results in the above solar cells, it is very important to control the size and the separation of the Pt particles on a

nanometer scale. The theoretical consideration predicts that the ideal size and separation are ca. 5 nm and ca. 20 nm, respectively [19, 20].

In the present work, the author has made detailed studies on the nanometer-scale control of the size and the separation of the Pt particles and its effect on the solar cell characteristics. The studies have been aimed at obtaining quantitative relations between the size and the separation of the Pt particles and the solar cell characteristics and verifying the theoretical prediction. Although the ultimate purpose of this work is to develop a high-efficiency and low-cost solid-state solar cell of Fig. 1(B)-type, the PEC cells equipped with single crystalline n-Si electrodes have been used in the present work because they are fabricated simply by immersing the n-Si electrode into a redox electrolyte solution, without any other procedures causing surface damages, and thus they are suitable for investigating the relations between the properties of the Pt particles and the solar cell characteristics.

In the first chapter, a simple method of dropping a solution of colloidal Pt particles on an n-Si electrode is used for the electrode preparation. The solutions of Pt colloid of 5 to 50 nm in diameter were prepared by various methods such as the use of commercially available Pt black, the microemulsion method, the extraction-reduction method, the alcohol-reduction method and Bredig's method. The V_{OC}'s of 0.550 to 0.630 V are obtained, independent of the size of the Pt particles. This result is explained by taking into account the presence of the nanometer-scale roughness of the n-Si surface. By use of n-Si electrodes with textured surfaces, modified with the Pt colloid particles prepared by Bredig's method, the solar energy conversion efficiency (AM1) of 14.9 % is obtained, which is the highest for the n-Si PEC solar cells ever reported.

In the second chapter, the Langmuir-Blodgett (LB) layers of Pt colloid particles are prepared for the first time and used for controlling the Pt-particle distribution

on n-Si on a nanometer scale. The Pt-particle density is successfully controlled by regulating the specific area of the Langmuir layer on a water surface. It is confirmed that the V_{OC} increases with decreasing Pt particle density and reaches 0.635 V at maximum.

In the third chapter, it is shown that the minority-carrier controlled (ideal) PEC solar cells are obtained in case where the n-Si electrodes are modified with the LB layers of the Pt-colloid particles at a small density. This indicates that an ideal n-Si/solution junction is obtained. The ideality factor (n) and the dark saturation current density (j_0) are determined from plots of logarithm of the short-circuit photocurrent density versus V_{OC}. It is found that n is unity for all the electrodes. As the Pt particle density is decreased and the post-heat-treatment temperature is lowered, the j_0 decreases and thus the V_{OC} increases. The decrease in j_0 is mainly caused by the decrease of the majority-carrier dark saturation current density (j_{0n}). For the n-Si electrodes modified with Pt at a small density and heat-treated at low temperature, the j_{0n} becomes lower than the minority-carrier dark saturation current density (j_{0p}), thus leading to the minority-carrier controlled solar cells.

In the fourth chapter, the structure and properties of porous n-Si electrodes coated with Pt are studied in detail. The porous n-Si electrodes, prepared by photoetching in hydrofluoric acid (HF), have macroporous layers, consisting of micrometer-sized pores and Si pillars. The wall and top of the Si pillars are further covered with nanoporous layers having nanometer-sized pores. The nanoporous layer can be thinned by immersion in HF. The solar cell characteristics are first improved by thinning the nanoporous layer, but reaches maxima, and then are worsened. A high conversion efficiency of 14.0 % is obtained. A new mechanism for obtaining high efficiencies by use of porous n-Si electrodes is discussed.

References

1) J. Zhao, A. Wang, P. Altermatt, and M. A. Green, *Appl. Phys. Lett.*, **66**, 3636 (1995).
2) S. R. Wenham and M. A. Green, *Prog. Photovolt., Res. Appl.*, **4**, 3 (1996).
3) M. A. Green, K. Emery, K. Bücher, and D. L. King, *Prog. Photovolt., Res. Appl.*, **4**, 59 (1996).
4) A. Rohatgi, Z. Chen, P. Sana, J. Crotty, and J. Salami, *Sol. Energy Mater. Sol. Cells*, **34**, 227 (1994).
5) C. R. Wronski, *Sol. Energy Mater. Sol. Cells*, **41/42**, 427 (1996).
6) J. E. Cotter, A. M. Barnett, D. H. Ford, R. B. Hall, A. E. Ingram, J. A. Rand, T. R. Ruffins, K. P. Shreve, and C. J. Thomas, *Prog. Photovolt., Res. Appl.*, **3**, 351 (1995).
7) A. Catalano, *Sol. Energy Mater. Sol. Cells*, **41/42**, 205 (1996).
8) K. Zweibel, *Prog. Photovolt., Res. Appl.*, **3**, 279 (1995).
9) H. Tsubomura and H. Kobayashi, *Cri. Rev. Solid State Mater. Sci.*, **18**, 261 (1993).
10) A. J. Nozik and R. Memming, *J. Phys. Chem.*, **100**, 13061 (1996).
11) B. O'Regan and M. Grätzel, *Nature*, **353**, 737 (1991).
12) A. Fujishima and K. Honda, *Nature*,**238**, 37 (1972).
13) R. C. Kainthla, B. Zelenay, and J. O'M. Bockris, *J. Electrochem. Soc.*, **134**, 841 (1987).
14) Y. Sakai, S. Sugahara, M. Matsumura, Y. Nakato, and H. Tsubomura, *Can. J. Chem.*, **66**, 1853 (1988).
15) K. Ueda, Y. Nakato, Y. Sakai, M. Matsumura, and H. Tsubomura, *J. Appl. Phys.*, **64**, 1513 (1988).

16) R. Hinogami, T. Mori, S. Yae, and Y. Nakato, *Chem. Lett.*, 1725 (1994).

17) H. Yoneyama, K. Sugimura, and S. Kuwabata, *J. Electroanal. Chem.*, **249**, 143 (1988).

18) R. Hinogami, Y. Nakamura, S. Yae, and Y. Nakato, *Appl. Surf. Sci.*, submitted.

19) Y. Nakato, K. Ueda, H. Yano, and H. Tsubomura, *J. Phys. Chem.*, **92**, 2316 (1988).

20) Y. Nakato and H. Tsubomura, *Electrochim. Acta*, **37**, 897 (1992).

21) Y. Nakato, K. Kai, and K. Kawabe, *Sol. Energy Mater. Sol. Cells*, **37**, 323 (1995).

22) S. Yae, J.-G. Jia, M. Fujitani, and Y. Nakato, *Tech. Digest Int'l PVSEC-9*, Miyazaki, Japan, p.511 (1996).

Chapter 1

Efficient Photoelectrochemical Solar Cells, Equipped with an n-Si Electrode Modified with Colloidal Platinum Particles

Introduction

Recent studies on single-crystal silicon (Si)-based p-n junction solar cells have shown that the solar energy conversion efficiency reaches 20 % or more by elaborating microstructures by photolithographic techniques [1-3]. However, it seems very difficult to apply such techniques to semiconductor materials such as polycrystalline thin films, which are expected to be the most promising materials for the fabrication of practical low-cost solar cells.

It is thus still important to develop new approaches to high-efficiency and low-cost solar cells. Lewis et al. reported an efficient (ϕ^S = 14.0 %) photoelectrochemical (PEC) solar cell using a single crystal n-Si electrode and a non-aqueous redox electrolyte solution [4]. We have been studying the solar cells of a new type [5-13], in which semiconductor wafers are modified with sparsely distributed ultrafine metal particles, the naked part of the semiconductor surface being covered with a passivating thin oxide layer.

Our recent experiments showed that the single crystal n-Si PEC solar cells of the above type gave the open-circuit photovoltages (V_{OC}) of 0.59 to 0.68 V [5-8], considerably higher than that (0.59 V) for the conventional p-n junction Si solid solar cells having nearly the same simple structure. The n-Si PEC cells have stability

sufficient for the laboratory-scale experiments, but unfortunately have no enough stability for long-term practical application. However, we can make stable solid-state solar cells of a structure "transparent conductor/ultrafine metal particles embedded in an oxide layer/semiconductor", by applying the principle and the techniques of the above n-Si PEC solar cells [5, 13]. Furthermore, the PEC cells of the present type equipped with p-type Si electrodes are stable because they are stable for photocathodic reactions, and can be used for direct conversion of solar energy into chemical energy such as hydrogen photoevolution [8-10] and carbon dioxide photoreduction [11].

Although we have obtained very high V_{OC}'s for the n-Si PEC cells of the present type, as mentioned above, the V_{OC} values are scattered from electrode to electrode, even for electrodes prepared in the same conditions. This is probably due to the scattering in the size and the separation of the metal particles on n-Si because they were not well controlled in the methods adopted thus far. Theoretical consideration has shown that it is very important to control the size and the separation of the metal particles on a nanometer scale for both the PEC and the solid-state solar cells, the ideal size and separation being estimated to be ca. 5 nm and about 20 nm, respectively [5, 7].

Thus, we have started studies for controlling the size and the separation of the metal particles by using the n-Si PEC cells, which are convenient for testing how well the metal particles are deposited because only immersing the n-Si electrode in the solution is enough to make the PEC cells. In the present work, we have prepared various colloidal platinum (Pt) solutions and applied them to n-Si.

Experimental

1. Preparation of Platinum Colloid Solutions.

Use of Commercially Available Pt Black: Commercial Pt black (N.E. Chemcat) and stearic acid (recrystallized from benzene solutions) or oleic acid were mixed and ground well in a mortar. The mixture was dispersed into benzene. The supernatant liquid was used as the Pt colloid solution.

Microemulsion Method [14]: 0.58 g of pentaethyleneglycol mono-n-dodecyl ether was dissolved in 10.69 g n-hexane. 33.2 mg water including 9.07 mg hexachloroplatinic(IV) acid was dispersed in this n-hexane solution, in the form of microemulsion through the formation of reversed micelles. Then, 0.025 cm^3 hydrazine monohydrate was added as a reductant. The color of the solution changed from light yellow to black as the reduction reaction proceeded.

Extraction-Reduction Method [15]: 10 cm^3 of an aqueous solution of 1.5×10^{-3} M (M = mol dm^{-3}) hexachloroplatinic(IV) acid and 50 cm^3 of a chloroform solution of 1.5×10^{-3} M dioctadecyldimethylammonium chloride (DDAC) were mixed and shaken for 12 h. The hexachloroplatinic(IV) acid was extracted by the surfactant (DDAC) into the chloroform solution, and it was reduced by refluxing at 65°C in the presence of formaldehyde, triethylamine and water under a nitrogen atmosphere. The solution turned dark brown in 1 h.

Alcohol-Reduction Method (Polymer-Stabilized Platinum Colloid Solutions) [16]: 3 mg of poly(N-vinyl-2-pyrrolidone) (PVP) was dissolved in 30 cm^3 of a 1-propanol solution of 0.5×10^{-3} M hexachloroplatinic(IV) acid. The solution was refluxed till it became black. As an alternative method, 20 cm^3 of water containing 6 mg

polyvinylalcohol (PVA) and 10 cm^3 of an ethanol solution of 3×10^{-3} M hexachloroplatinic(IV) acid were mixed and refluxed.

Bredig's Method [17]: Two platinum wires, between which a DC voltage of 35 V was applied, were patted together repeatedly for about 10,000 times in ethanol, till it became dark grayish. The platinum colloid solution thus obtained contained 0.1 ~ 0.2 mg cm^{-3} platinum.

2. Preparation of n-Si Electrodes and Deposition of Platinum Colloid Particles.

Single crystal n-Si wafers [Shin-Etsu Handotai Co., Ltd., CZ, (100), $\rho = 0.7$ ~ 1.3 Ωcm, $N_D = (3 \sim 7) \times 10^{15}$ cm^{-3} as estimated from the ρ values using Fig. 21 of chapter 1 of ref. 18, 0.4 ~ 0.7 mm thick, and (111), 0.4 ~ 0.9 Ωcm, 0.605 mm thick] were cut into small pieces (0.6 ~ 0.7 cm^2). Textured Si surfaces were produced by the immersion of the Si pieces successively in a 4 M sodium hydroxide (NaOH) solution at 85°C and in a (0.25 M NaOH + 0.6 M 2-propanol) solution at 85°C [19]. The flat- and textured-surface n-Si pieces were washed with boiled acetone and water, etched in a 33 % CPD-2 [a mixture of nitric acid (HNO_3), hydrofluoric acid (HF) and bromine (1:1:0.001 in volume)], and finally etched again with 1 or 12 % HF.

The deposition of platinum colloid particles on n-Si was performed by dropping $3 \sim 50 \times 10^{-3}$ cm^3 platinum colloid solutions on the n-Si pieces, followed by drying in vacuum. In some cases, the n-Si pieces thus modified were heated at 300°C under vacuum (~ 1.3×10^{-4} Pa) or a stream of hydrogen for 10 min in order to obtain good solar cell characteristics.

3. Current Density (j) vs. Potential (U) Measurements.

Ohmic contacts were made on the rear side of the n-Si pieces with indium-gallium alloy. The n-Si piece, having the Pt colloid on the front side, was placed in a Teflon holder (effective area: 0.25 cm^2) [19] and used as an n-Si electrode for photoelectrochemical measurements. A platinum plate was used as the counterelectrode, and an aqueous solution of 8.6 M hydrogen bromide (HBr) and 0.02 ~ 0.05 M bromine (Br_2) was used as the redox electrolyte. Deionized water and reagent-grade chemicals were used for all the experiments.

Photocurrent density (j) vs. potential (U) curves were obtained with a potentiostat and a potential programmer. The electrolyte solution was stirred magnetically during the measurements. The potential of the n-Si electrode was measured with respect to the counterelectrode. An AM1 100 $mWcm^{-2}$ solar simulator (WXS-85H, Wacom) was used as the light source.

The Pt colloid particles on n-Si were inspected with a scanning electron microscope (ALPHA-30A, Akashi-Seisakusyo). X-ray diffraction (XRD) patterns were measured with a Rigaku Model RAD-ROC X-ray diffractometer and a Shimadzu VD-1 X-ray diffractometer. X-ray photoelectron spectroscopic (XPS) analysis was performed with Shimadzu ESCA-750 and ESCA-1000 spectrometers with MgK_α X-ray sources. Light transmittance spectra of the redox solutions were recorded with a Shimadzu UV-360 spectrophotometer. Photocurrent action spectra were measured using a monochromator (MC-50, Ritsu Oyokogaku) and a 500 W Xe-lamp (Ushio).

Results

Figure 1 shows the j-U curves for the PEC solar cells, equipped with the n-Si electrodes modified with Pt colloid particles prepared by Bredig's method. The curves a and b are for textured- and flat-surface n-Si electrodes, respectively. By the formation of the textured surface, the V_{OC} was decreased from 618 mV to 597 mV,

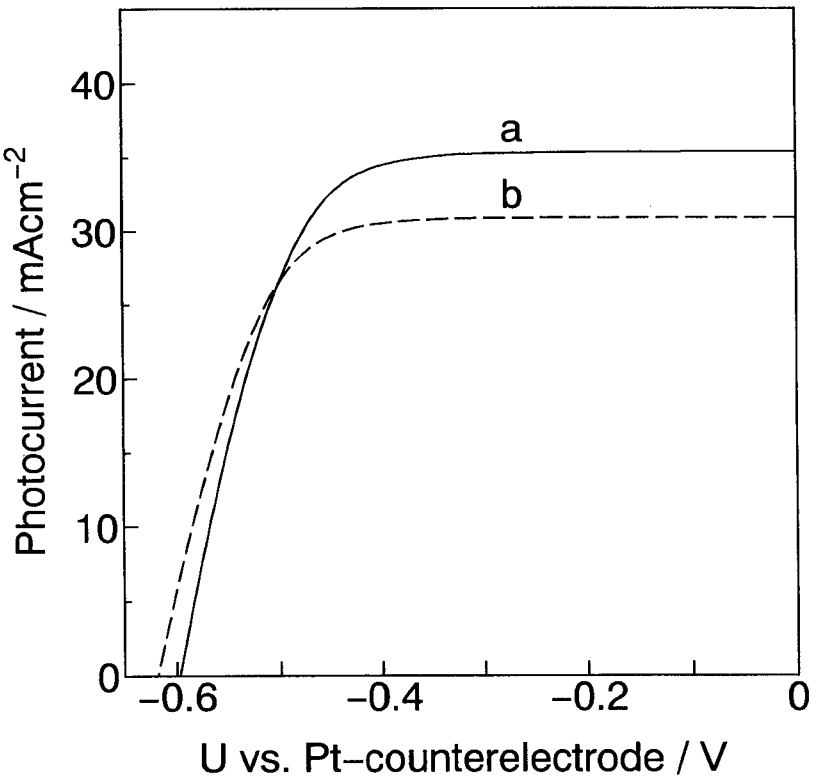

Figure 1. Photocurrent density (j) vs. potential (U) curves for the PEC cells equipped with the n-Si electrodes modified with the Bredig's-method Pt particles in a 8.6 M HBr + 0.025 M Br_2 aqueous solution under simulated solar AM1 100 mWcm^{-2} illumination. The curves a and b are for textured- and flat-surface n-Si electrodes, respectively.

but the short-circuit photocurrent density (j_{SC}) was increased from 30.9 $mAcm^{-2}$ to 35.4 $mAcm^{-2}$ as calculated from the apparent surface area of the electrode. Thus, the solar energy conversion efficiency (ϕ^S) for the textured-surface electrode (curve a of Fig. 1) reached 14.9 %.

Table 1 summarizes characteristics of the PEC solar cells equipped with the n-Si electrodes modified with various Pt colloid particles. All the Pt particles prepared in the present work gave V_{OC}'s of 0.550 to 0.630 V, which are much higher than those (0.25 ~ 0.30 V) for the PEC cells equipped with n-Si electrodes coated with continuous Pt layers (0.1 ~ 3 nm thick) by the electron-beam evaporation method [7]. Of the various n-Si electrodes, the n-Si electrodes modified with Pt particles prepared by Bredig's method yielded the highest fill factors (F.F.) on the average.

Figure 2 shows scanning electron micrographs (SEM) for the microemulsion-method Pt particles (A) and the Bredig's-method Pt particles (B) dropped on n-Si. The Pt particles (white parts of the micrographs) in both the electrodes aggregate with each other, forming fairly large islands, and are rather inhomogeneously distributed. The average diameters of the Pt particles were calculated from the width at the half height of the XRD peaks, Pt <100> (2θ = 39.8°) and Pt <200> (2θ = 46.3°), by using Scherrer's equation [20]. The results are listed in Table 1. The diameters thus obtained from the XRD peaks were much smaller than the size of the Pt islands in the SEM (Fig. 2).

Figure 3 shows the spectral response curve (A) for the n-Si electrode modified with the Bredig's-method Pt particles, as compared with the light transmittance spectra (B) of 8.6 M HBr + 0.025 and 0.05 M Br_2 solutions. In Fig. 3B, two depressions at wavelengths λ = 1190 nm and 970 nm are due to the vibrational overtone bands of water [21]. The depression in wavelengths shorter than 560 nm

Table 1. The open-circuit photovoltage (V_{OC}), the short-circuit photocurrent density (j_{SC}) and the fill factor (F.F.) for the PEC solar cells equipped with the n-Si electrodes modified with various Pt colloid particles, at temperatures of 15 to 25 °C under simulated solar AM1 100 $mWcm^{-2}$ illumination. All the values are for the initial stage of measurements.

Methods of preparation of Pt particles	d[a] (nm)	No. of tested samples	V_{OC}[b] (V)	j_{SC}[b] ($mAcm^{-2}$)	F.F.[b]	ϕ^S[b] (%)	Remarks[c]
Commercial Pt-black	8-14						
stearic acid stabilized		3	0.600 - 0.615 (0.609)	17.6 - 22.4 (19.7)	0.658 - 0.699 (0.665)	7.2 - 9.6 (8.1)	Ox1, HT1, C1
		6	0.580 - 0.600 (0.585 ± 0.010)	17.7 - 24.0 (22.1 ± 2.1)	0.591 - 0.709 (0.677 ± 0.040)	6.9 - 9.6 (8.7 ± 1.0)	HF2, C1
oleic acid stabilized		7	0.595 - 0.620 (0.603 ± 0.008)	21.5 - 24.9 (22.7 ± 1.1)	0.664 - 0.743 (0.698 ± 0.029)	8.7 - 10.3 (9.6 ± 0.6)	HF1, HT1, C1
Microemulsion	8-22	3	0.600 - 0.617 (0.609)	20.5 - 21.9 (21.0)	0.613 - 0.681 (0.640)	7.8 - 8.5 (8.2)	Ox2, HT1, C1
		6	0.550 - 0.598 (0.572 ± 0.017)	22.9 - 27.8 (25.7 ± 1.8)	0.643 - 0.708 (0.681 ± 0.023)	8.7 - 11.0 (10.2 ± 0.5)	HF1, HT1, C3
Extraction-reduction	15-32	8	0.593 - 0.608 (0.602 ± 0.005)	24.5 - 28.6 (25.8 ± 1.4)	0.505 - 0.631 (0.573 ± 0.033)	8.0 - 10.2 (8.9 ± 0.8)	Ox2, HT1, C3, F
Alcohol reduction	~ 5						
PVP-stabilized		4	0.610 - 0.625 (0.616 ± 0.006)	25.8 - 27.5 (27.1 ± 0.3)	0.550 - 0.606 (0.577 ± 0.020)	9.1 - 10.0 (9.6 ± 0.3)	HF2, C1
PVA-stabilized		5	0.610 - 0.630 (0.618 ± 0.010)	21.6 - 25.6 (23.5 ± 1.5)	0.679 - 0.709 (0.688 ± 0.011)	9.0 - 10.6 (10.0 ± 0.6)	HF2, C1
Bredig	14-50	36	0.570 - 0.620 (0.601 ± 0.013)	23.0 - 29.3 (25.8 ± 1.6)	0.546 - 0.757 (0.702 ± 0.083)	8.0 - 12.8 (11.0 ± 1.0)	HF2, C1
		4	0.610 - 0.627 (0.619 ± 0.006)	26.5 - 27.9 (27.2 ± 0.6)	0.687 - 0.753 (0.732 ± 0.026)	11.7 - 12.8 (12.3 ± 0.4)	Ox3, C1
		9	0.565 - 0.620 (0.592 ± 0.016)	23.0 - 27.9 (25.4 ± 1.5)	0.695 - 0.748 (0.724 ± 0.018)	10.1 - 11.8 (10.9 ± 0.6)	Ox1, HT2, C1
		5	0.592 - 0.602 (0.596 ± 0.003)	32.0 - 35.4 (34.7 ± 1.4)	0.650 - 0.709 (0.690 ± 0.021)	13.4 - 14.9 (14.2 ± 0.6)	HF2, C2, S

(Table 1, continued on P. 19)

(Table 1, continued from p. 18)

a) The average diameter of the Pt particles estimated from the XRD peaks (see text), except the value for D which is estimated by the transmission electron microscopy.

b) The lowest and highest values are indicated, together with the average value and the standard deviation in parentheses. The ϕ^S values for the cells indicated in the lowest row are 13.4, 14.0, 14.1, 14.8, and 14.9.

c) HF1 and HF2: The n-Si electrodes were etched with 1 % HF for 30 ~ 60 min and with 12 % HF for 2 min, respectively, before dropping the Pt colloid solutions. Ox1, Ox2 and Ox3: The n-Si surfaces were slightly oxidized by immersing in 63 % HNO_3 for 10 min, in 63 % HNO_3 for 20 s, and in 5 M HNO_3 for 20 s, respectively, all at 20 ~ 25°C, before dropping the Pt colloid solutions. HT1 and HT2: The n-Si electrodes were heat-treated at 300°C for 10 min under H_2 or vacuum, respectively, after the dropping of the Pt colloid solutions. C1, C2 and C3: The Br_2 concentration of the electrolyte was 0.05, 0.025 and 0.02 M, respectively, the HBr concentration being 8.6 M in all the cases. F: The n-Si [CZ, (111), 0.4 ~ 0.9 Ωcm] wafers were used only for this case, though the n-Si [CZ, (100), 0.7 ~ 1.3 Ωcm] wafers were used in all the other cases. S: The textured-surfaces electrodes were used only for this case, though the flat-surface electrodes were used in all the other cases.

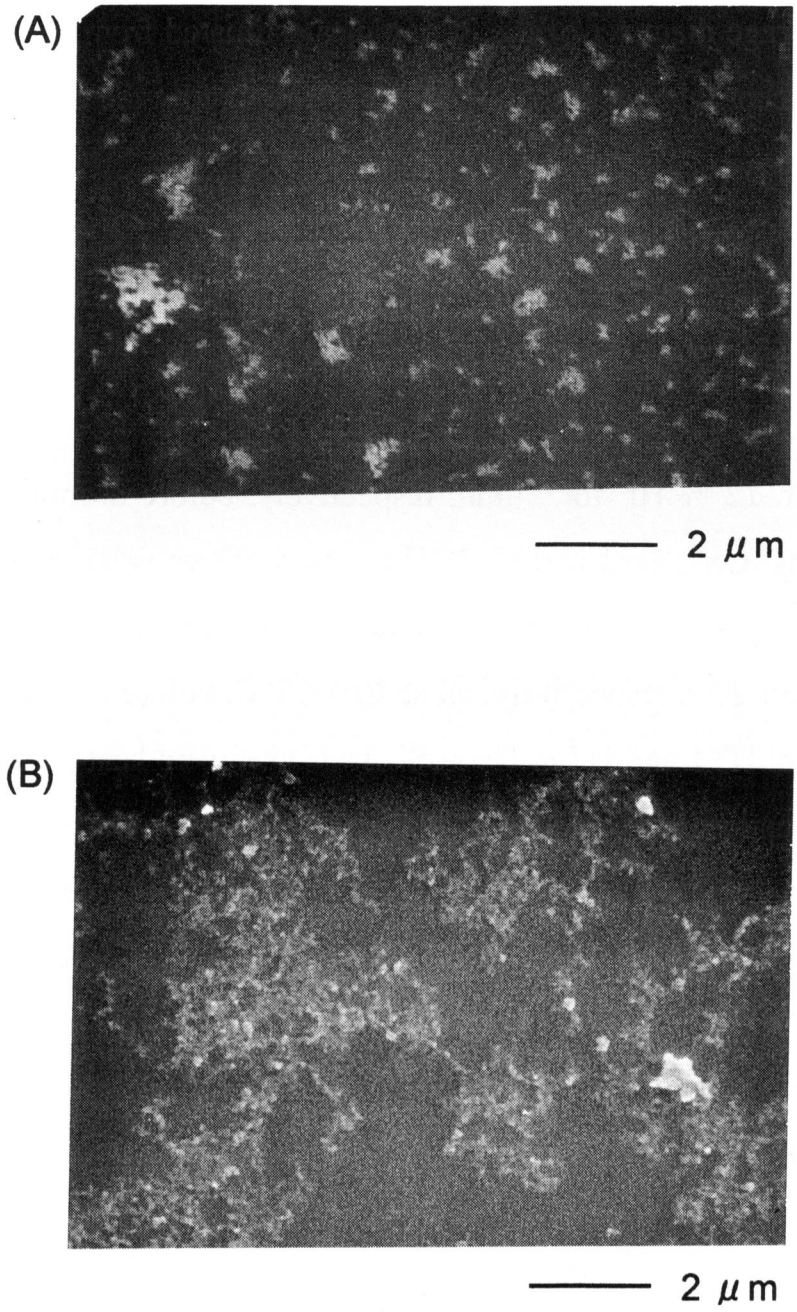

Figure 2. Scanning electron micrographs for the microemulsion-method Pt particles (A) and the Bredig's-method Pt particles (B) dropped on n-Si. The electrodes (A) and (B) in this figure were made by the same conditions as the second row of B and the first row of E in Table 1, respectively.

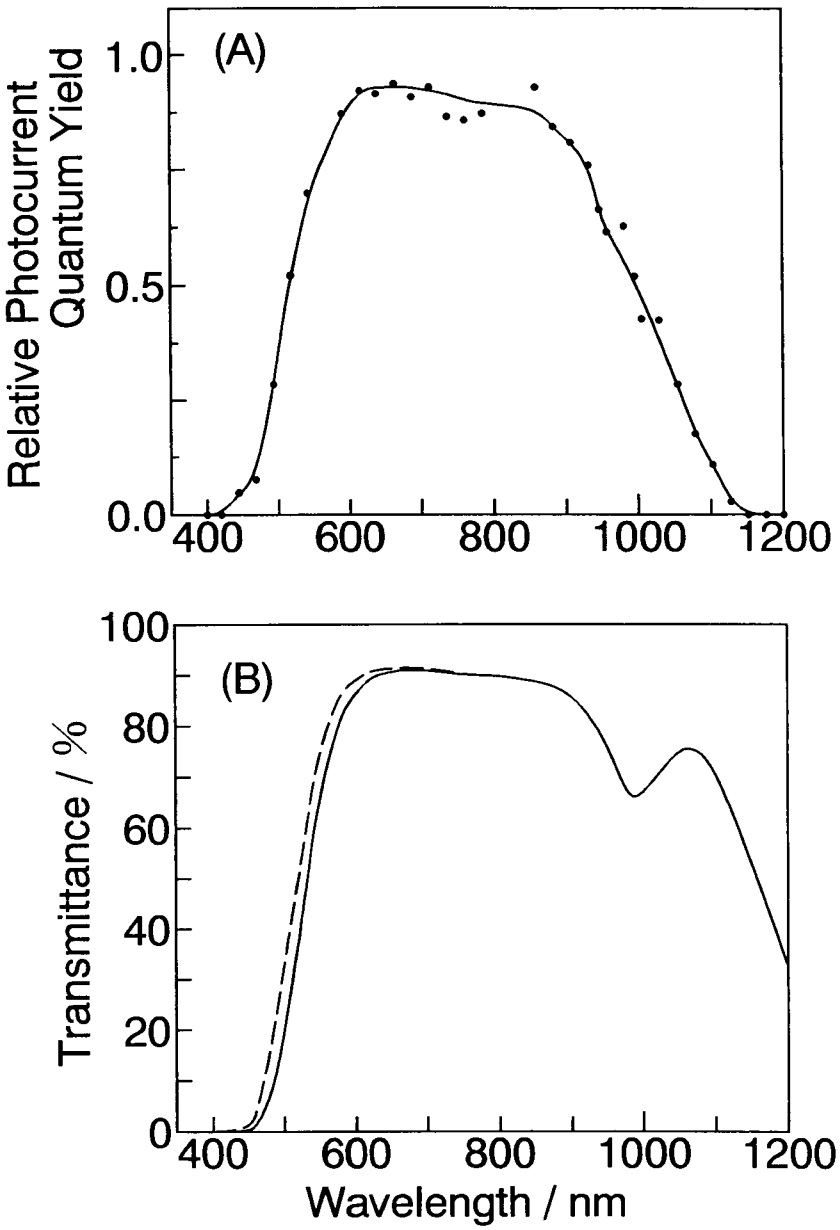

Figure 3. (A): Relative photocurrent quantum yields vs. wavelength for the n-Si electrode modified with the Bredig's-method Pt particles in a 8.6 M HBr + 0.05 M Br_2 aqueous solution. The thickness of the solution layer between the electrode surface and the glass window is 5 mm. (B): The transmittance spectra of 8.6 M HBr + 0.05 M Br_2 (solid line) and 8.6 M HBr + 0.025 M Br_2 (broken line) solutions. The optical path length is 10 mm.

is due to the absorption of bromine, and thus depends on the Br_2 concentration. The light transmittance of a layer of the Bredig's-method Pt particles on a glass plate, prepared by dropping the Pt colloid solution in the same Pt density (8×10^{-6} g Pt per 0.64 cm^2) as for the n-Si electrodes, was 93 % to 97 % in the wavelength range from 450 nm to 1100 nm. This is much higher than that (66 % to 73 %) for a 3.4 nm-thick continuous Pt film (4.7×10^{-6} g/0.64 cm^2) made by the electron-beam evaporation method.

The j-U curves for the Pt-particle modified n-Si electrodes such as shown in Fig. 1 were unchanged during several cyclic potential scans for 1 to 10 min. There was a tendency that the stability was improved by the increase in the amount of the deposited Pt particles. On the other hand, the photocurrents for naked n-Si electrodes in the HBr/Br_2 solution at 0 V vs. Pt counterelectrode quickly decayed to 0.00 $mAcm^{-2}$ within 15 s after start of illumination, clearly showing typical passivation behavior. XPS analysis of the passivated electrodes showed the formation of thin silicon oxide layers about 1.3 nm thick as estimated on the basis of the mean free path (2.5 nm) of Si2p photoelectrons (1150 - 1155 eV) in silicon oxide [22, 23].

The stability of the Pt-particle modified n-Si electrodes in general increased by the heat-treatments at 300°C under H_2 or vacuum for 10 min after the Pt-particle deposition, although unfortunately the V_{OC} values were reduced by 0.02 to 0.05 V by the heat-treatments. For the n-Si electrode modified with the Bredig's method Pt particles and heat-treated, the V_{OC} decreased from 0.58 V (initial value) to 0.54 and 0.49 V by continuous illumination at -0.4 V vs. Pt counterelectrode for 60 and 3180 min, respectively. The F.F. also decreased from 0.72 to 0.70 and 0.56 in the same experiment, but the j_{SC} of ~ 25 $mAcm^{-2}$ was kept unchanged. Similar results were obtained for other three electrodes. The best stability data were obtained for

the n-Si electrode first covered with a 1.1-nm thick surface oxide layer by dipping in 63 % HNO_3 for 10 min and coated with the Bredig's-method Pt particles, followed by the heat-treatment in vacuum. The V_{OC} of 0.58 V was kept constant under continuous 2 h-illumination at -0.4 V and decreased to 0.56 V after the 8 h-illumination.

The SEM inspection before and after the stability tests showed no change of the deposited Pt, indicating that no Pt is dissolved. The XPS analysis also showed no decrease in the amount of the deposited Pt. These results, i.e., no dissolution of the Pt particles together with the passivation behavior of the naked n-Si surface, strongly suggest that the photocurrents for the Pt-particle modified n-Si electrodes are due to the redox reaction of the HBr/Br_2 couple, not due to the photocorrosion of the electrodes.

Figure 4 shows the Si2p XPS spectra for the Pt-particle modified n-Si electrodes. The 99-eV peak is assigned to the Si2p peak from bulk Si, while the 103-eV peak is assigned to that from surface Si oxide [22, 23]. The thickness of the surface Si-oxide layers, estimated from these spectra by the aforementioned method, was nearly equal to or thinner than 0.4 nm for the as-prepared electrodes, but it became thicker to 1.0 ~ 1.3 nm after the heat-treatment probably due to thermal oxidation of the Si surface by a small amount of contaminating oxygen in the ambient in the heat-treatment experiments. The oxide layers for the as-prepared electrodes also became thicker to 1.0 ~ 1.3 nm after the measurements of the j-U curves or the stability tests most probably due to Br_2-induced chemical oxidation and photoelectrochemical oxidation in the aqueous electrolyte. However, the oxide layers of the heat-treated electrodes no longer grew by the electrochemical measurements.

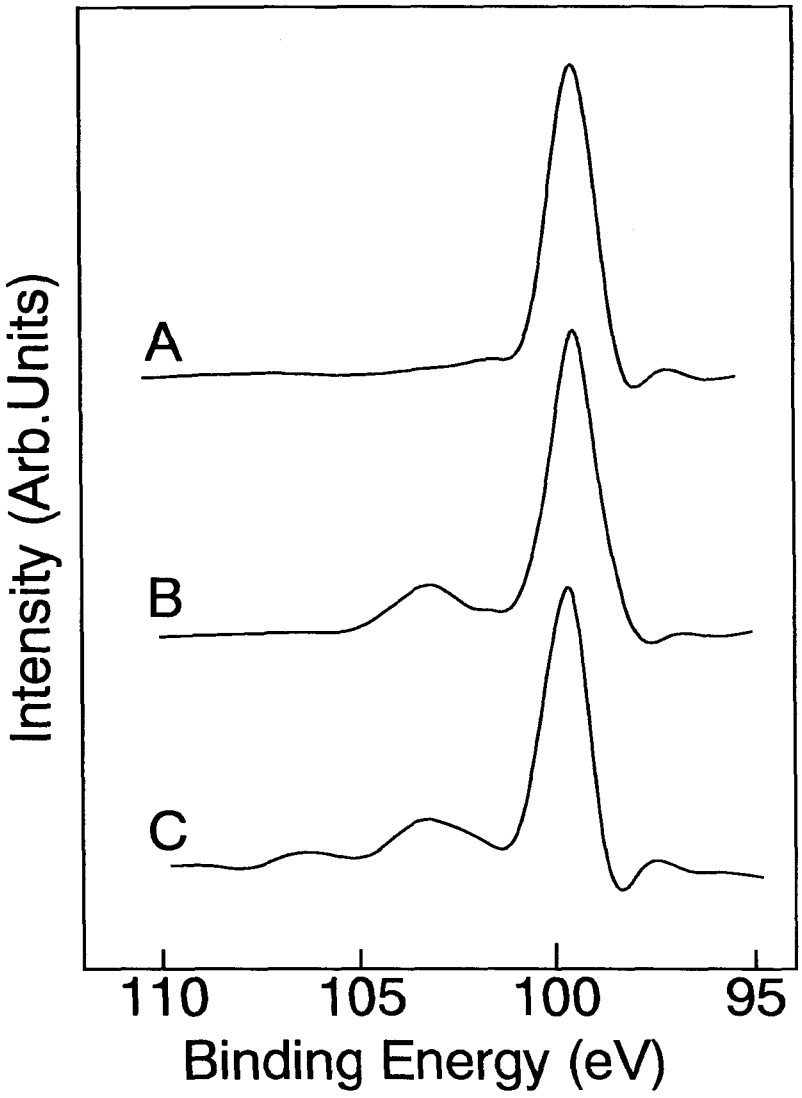

Figure 4. XPS spectra in the Si2p region for the Bredig's-method Pt-particle modified n-Si electrodes: (a) the as-prepared electrode, (b) the electrode heat-treated at 300°C in H_2 for 10 min after the Pt-particle deposition, and (c) the electrode without the heat-treatment but after the 30-min stability test.

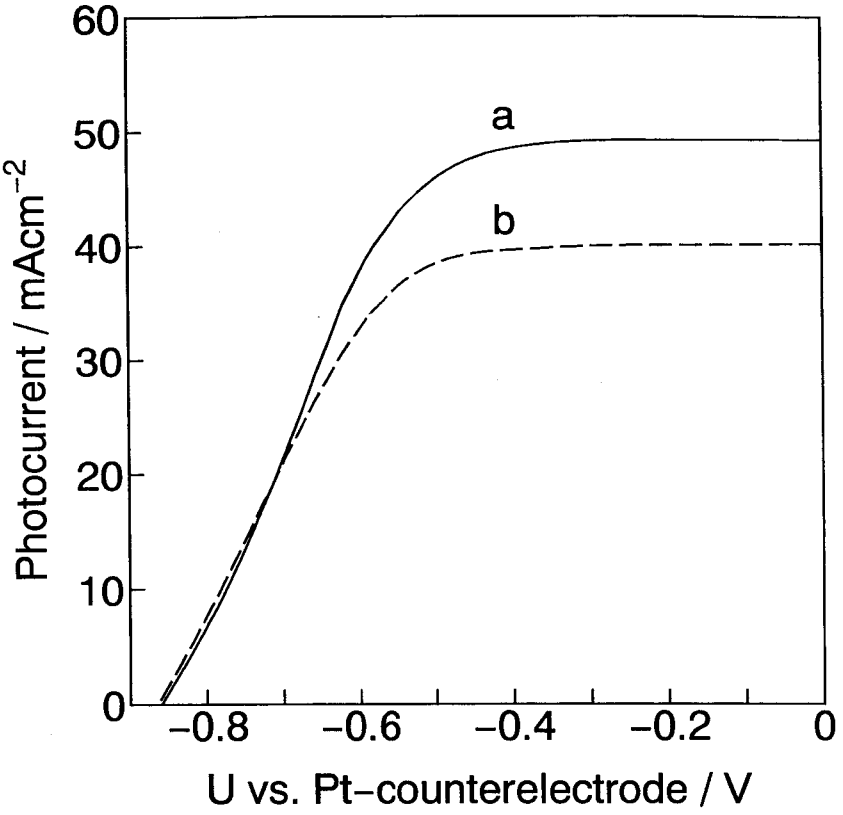

Figure 5. The j - U curves for the naked (a) and the Bredig's-method Pt-particle modified (b) n-Si electrodes in a 6.7 M HBr/0.04 M Br_2 aqueous solution containing 1.0 % HF. The electrolyte solution was stirred magnetically during the measurements.

In order to further confirm the above-mentioned argument that the photocurrents for the Pt-particle modified n-Si electrodes such as shown in Fig. 1 and Table 1 are not due to the electrode photocorrosion, we measured the j-U curves by using an aqueous 6.7 M HBr/ 0.04 M Br_2 solution containing 1.0% hydrogen fluoride (HF), in which n-Si can really photocorrode because the passivating silicon

oxide layer is dissolved by HF. Figure 5 shows the j-U curves obtained for the naked and the Pt-particle modified n-Si electrodes. Interestingly, both the electrodes showed nearly the same curves, contrary to the case of the HBr/Br_2 solution containing no HF where the naked n-Si electrode is completely passivated. Moreover, the apparent V_{OC} values reached 0.85 V and the short-circuit photocurrent density reached 40 $mAcm^{-2}$ or more, both are much higher than the values in Fig. 1, clearly indicating the behavior of photocorroding n-Si electrodes. The large j_{SC} value can be explained by taking account of the current-doubling mechanism in the photocorroding processes [24, 25]. Such apparently high V_{OC} and j_{SC} values were obtained also in the solutions containing much smaller amounts of HF, though the j_{SC} rapidly decreased with cyclic potential scanning.

The SEM showed that a large number of etch pits were formed on the n-Si surface after the experiments of Fig. 5, contrary to the case of experiments in the absence of HF. Also, the XPS analysis indicated that 90 % or more of the deposited Pt, as calculated from the atomic Pt/Si ratio, was removed after the experiment of Fig. 5, suggesting that the deposited Pt is detached from the electrode surface in case where the electrode corrosion occurs. These results, as compared with the results obtained for the HBr/Br_2 solution containing no HF, confirm that the photocurrents of Fig. 1 and Table 1 are not due to the electrode photocorrosion. The same argument was given in our previous papers [7, 8] by showing that the observed V_{OC} values strongly depended on the size and the separation of the Pt particles (or islands) in such a manner as expected by our theory [5, 8], which could not be explained by the photocorrosion mechanism.

Discussion

The n-Si electrodes modified with the Pt colloid particles, prepared in the present work, gave high V_{OC}'s of 0.550 to 0.630 V (Table 1). These values can be explained [5, 7] if we calculate the majority-carrier component (j_{0n}) of the dark saturation current density by modifying the thermionic emission theory [18] and the minority-carrier component (j_{0p}) by using Shockley's bulk diffusion-recombination theory [18] with the minority carrier diffusion length for n-Si (Shin-Etsu Handotai, CZ, ρ ~ 1 Ωcm) taken to be 110 ~ 120 μm [26], provided that the areas of the Pt-Si contacts are small enough. However, some discussion is necessary for the last condition because the SEM showed that the Pt particles on n-Si aggregate with each other, forming large islands 0.1 to 1 μm in diameter. This size is much larger than the ideal size (~ 5 nm) estimated theoretically [7]. The size of the Pt particles themselves, estimated from the widths of the XRD peaks, is also fairly large, ranging from 8 to 50 nm (Table 1).

The above result can be explained by taking into account a model of Fig. 6. The Pt particles are expected to be spherical in shape, whereas it is reported by STM observations [27, 28] that the HF-etched Si surface is atomically rough, showing a rolling hill structure in the 5 to 20-nm scale range. Thus, the areas of direct Pt-Si contacts (thick black part in Fig. 6) should be much smaller than the diameter of the Pt particles. The situation is unchanged even if the Pt particles aggregate because the electrolyte solution can penetrate into the openings between the Pt particles and the n-Si surface. All the n-Si surface, except the direct Pt-Si contacts, is covered with a thin silicon oxide layer and passivated, as indicated by the j-U curve measurements and the XPS analysis. Moreover, such oxidation of the n-Si surface may proceed even in the margins of the areas of the direct Pt-Si contacts when the

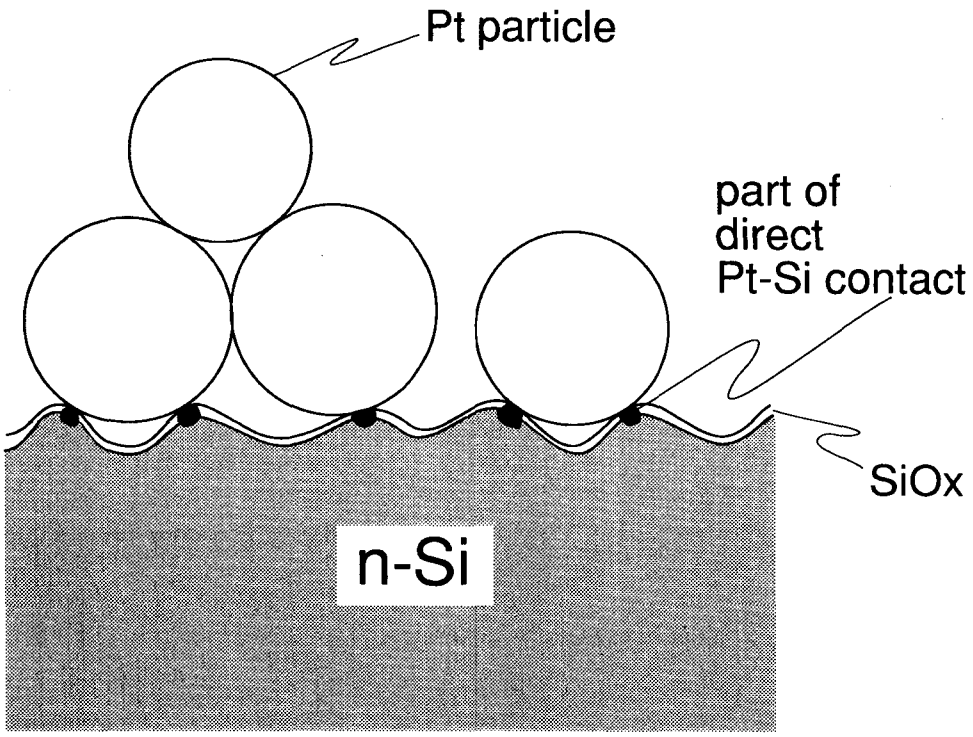

Figure 6. Schematic cross section of the n-Si electrode modified with the Pt colloid particles.

electrodes are immersed and illuminated in the strongly oxidizing HBr/Br_2 aqueous solution, which makes the areas of the direct Pt-Si contacts further narrower. It is thus not unreasonable to assume that the effective width of the direct Pt-Si contacts that cause the energy band modulation at the n-Si electrode [7] is around 5 nm.

The oxidation of the n-Si surface in the margins of the areas of the direct Pt-Si contacts may bring the beneficial effect on the V_{OC} as mentioned above, but it is likely that this oxidation leads to the gradual degradation of the Pt-particle modified

n-Si electrodes as mentioned in the preceding section. The improvement in the stability by the heat-treatments can be explained by the formation of chemically firm Pt-Si contacts, probably accompanied by slight silicide formation as suggested by our XPS analysis. The similar argument was reported in our previous paper [8]. The slight decrease in V_{OC} by the heat-treatments can be explained also in terms of silicide formation which leads to the increase in the areas of the direct Pt-Si (or Pt silicide-Si) contacts.

The highest F.F. was obtained on the average for the n-Si electrodes modified with the Bredig's-method Pt particles (Table 1). The result can be explained as follows. The Pt particles prepared by Bredig's method are negatively charged in ethanol, and dispersed by the electrostatic repulsion without any surfactant or polymer as a stabilizer. Thus, when this Pt solution is dropped on the n-Si surface and dried in vacuum, the Pt particles can make direct contact with n-Si. On the other hand, the Pt colloid solutions prepared by the other methods contain surfactants or polymers as stabilizers. When such a solution is dropped on n-Si and dried, the Pt particles are covered with the surfactants or polymers, which hinder the formation of the direct Pt-Si contacts and decrease the hole transfer rate from n-Si to Pt. This leads to the lowering of the F.F. In such cases, the heat treatment under vacuum or a stream of hydrogen is necessary to obtain high F.F., as really observed experimentally. The XPS analysis for the C1s peak showed that most of the surfactants are removed by the heat-treatments in H_2.

The PEC cells equipped with the textured-surface n-Si electrodes, modified with the Bredig's-method Pt particles, yielded the highest solar energy conversion efficiency (ϕ^S) of 14.9 % in the present work. By making the textured surface, the j_{SC} as calculated from the apparent electrode surface area was largely increased, but the V_{OC} and the F.F. were decreased (Fig. 1). The increase in j_{SC} is explained by

an increase in the light intensity absorbed by the semiconductor due to a decrease in the reflectivity for the textured n-Si surface [19, 29]. The decreases in V_{OC} and F.F. by the formation of the textured surface were observed also in our previous work [5, 8], where the Pt-islands were deposited by the method of coating with a H_2PtCl_6 solution and reduction under hydrogen at 320°C. The decrease in V_{OC} can be explained as being due to the increase in the real surface area for the textured n-Si electrode, which causes the increase in the majority-carrier dark saturation current density (j_{0n}) arising from the thermionic emission of the conduction-band electrons in n-Si to the Pt particles. If it is assumed that the Pt particles are well dispersed on the textured n-Si surface, the j_{0n} should increase with increasing the real surface area. The decrease in F.F. may be ascribed to the centering of the photocurrent near the top of the Si pyramids of the textured n-Si surface, to which the Br^- ions in the bulk of the solution can diffuse first. This will make the local photocurrent density near the top of the Si pyramids very high and lead to an increase in the potential drop at the Si/solution interface, resulting in the decrease in F.F.

References

1) R. A. Sinton, Y. Kwark, J. Y. Gan, and R. M. Swanson, *IEEE Electron Device Lett.*, **EDL-7**, 567 (1986).
2) A. Wang, J. Zhao, and M. A. Green, *Appl. Phys. Lett.*, **57**, 602 (1990).
3) M. A. Green and K. Emery, *Prog. Photovolt., Res. Appl.*, **1**, 25 (1993).
4) J. F. Gibbons, G. W. Cogan, C. M. Gronet, and N. S. Lewis, *Appl. Phys. Lett.*, **45**, 1095 (1984).
5) Y. Nakato and H. Tsubomura, *Electrochim. Acta*, **37**, 897 (1992).

6) Y. Nakato, H. Yano, and H. Tsubomura, *Chem. Lett.*, 987 (1986).

7) Y. Nakato, K. Ueda, H. Yano, and H. Tsubomura, *J. Phys. Chem.*, **92**, 2316 (1988).

8) K. Ueda, Y. Nakato, N. Suzuki, and H. Tsubomura, *J. Electrochem. Soc.*, **136**, 2280 (1989).

9) Y. Nakato, H. Yano, S. Nishiura, T. Ueda, and H. Tsubomura, *J. Electroanal. Chem.*, **228**, 97 (1987).

10) H. Kobayashi, F. Mizuno, Y. Nakato, and H. Tsubomura, *J. Phys. Chem.*, **95**, 819 (1991).

11) R. Hinogami, T. Mori, S. Yae, and Y. Nakato, *Chem. Lett.*, 1725 (1994).

12) S. Yae, Y. Nakato, M. Matsumura, Y. Sakai, and H. Tsubomura, *Nippon Kagaku Kaishi*, 1152 (1988).

13) Y. Nakato, S. Nishiura, H. Oshika, and H. Tsubomura, *Jpn. J. Appl. Phys.*, **28**, L261 (1989).

14) M. Boutnnet, J. Kizling, P. Stenius, and G. Maire, *Colloids Surf.*, **5**, 209 (1982).

15) K. Meguro, M. Torizuka, and K. Esumi, *Bull. Chem. Soc. Jpn.*, **61**, 341 (1988).

16) H. Hirai, Y. Nakao, and N. Toshima, *J. Macromol. Sci.-Chem.*, **A12**, 1117 (1978); H. Hirai, Y. Nakao, and N. Toshima, *J. Macromol. Sci.-Chem.*, **A13**, 727 (1979).

17) G. Bredig, *Z. Angew. Chem.*, **11**, 951 (1898); G. Bredig, *Z. Physik. Chem.*, **32**, 127 (1900).

18) S. M. Sze, *Physics of Semiconductor Devices*, 2nd ed., Wiley, New York, (1981).

19) K. Ueda, Y. Nakato, and H. Tsubomura, *Solar Energy Mater.*, **17**, 37 (1988).

20) P. Scherrer, Nachr. *Kgl. Ges. Wiss. Göttingen Math.-phys. Kl.*, 98 (1918).

21) H. Tsubomura, N. Yamamoto, N. Matsuo, and Y. Okada, *Proc. Jpn. Acad.*, **56**(B), 403 (1980).

22) H. Kobayashi, T. Ishida, Y. Nakato, and H. Tsubomura, *J. Appl. Phys.*, **69**, 1736 (1991).

23) F. J. Himpsel, F. R. McFeely, A. Taleb-Ibrahimi, and J. A. Yarmoff, *Phys. Rev. B*, **38**, 6084 (1988).

24) M. Matsumura and S. R. Morrison, *J. Electroanal. Chem.*, **144**, 113 (1983).

25) H. Gerischer and M. Lübke, *Ber. Bunsenges. Phys. Chem.*, **91**, 394 (1987).

26) The values were measured by the EBIC method in our laboratory.

27) E. Tomita, N. Matsuda, and K. Itaya, *J. Vac. Sci. Technol.*, **A8**, 534 (1990); K. Itaya, R. Sugawara, Y. Morita, and H. Tokumoto, *Appl. Phys. Lett.*, **60**, 2534 (1992).

28) C. F. Quate, *Surf. Sci.*, **299/300**, 980 (1994).

29) M. A. Green, *High Efficiency Silicon Solar Cells*, Trans Tech SA, Switzerland, (1987).

Chapter 2

Preparation of a Langmuir-Blodgett Layer of Ultrafine Platinum Particles and Its Application to n-Si for Efficient Photoelectrochemical Solar Cells

Introduction

The main target in recent solar-cell researches lies in how to fabricate low-cost solar cells without lowering the conversion efficiency. Many studies have been made toward this aim, mostly using polycrystalline thin films of Si [1-5], CdTe/CdS [6], $CuInSe_2$ [6], or granular Si [7] for solid-state solar cells. Various types of photoelectrochemical (PEC) solar cells have been studied, using single crystal Si [8], polycrystalline FeS_2 [9], dye-modified polycrystalline TiO_2 [10], among others.

We have been studying solar cells of a new type, for both PEC and solid-state application, in which a Si semiconductor is modified with ultrafine metal particles [11-18]. PEC solar cells of this type, with single crystal n-Si electrodes, generate extremely high open-circuit photovoltages (V_{OC}) of 0.62 to 0.685 V [12-16], and conversion efficiencies up to 14.9 % [16]. Though the n-Si PEC cells have inadequate stability for long-term practical application, the principle and the fabrication techniques can be applied to stable solid-state solar cells of the same type [11, 18]. The method is also expected to be applicable to polycrystalline Si thin films.

A continuing problem for the above-type solar cells is that, though the n-Si PEC cells give very high V_{OC}'s as mentioned above, the V_{OC} values are scattered

from electrode to electrode in the range of ± 0.02 V, for ostensibly similar preparations. This is probably due to scatter in the size and the separation of the metal particles on n-Si for the metal-particle deposition methods adopted thus far. Theoretically, it is of key importance for obtaining high V_{OC}'s to control the size and the separation of the metal particles on Si on a nanometer scale, the ideal size and separation for n-Si of 1 Ωcm being estimated to be about 5 nm and ca. 20 nm, respectively [12]. To control the metal particles on Si on such an ultrafine scale is quite difficult at present. It is impossible to attain it by use of the present photolithographic techniques. However, such ultrafine control is an interesting and challenging target because growing attention has recently been paid to developments of mesoscopic (or nanometer-scale) devices in the fields of electronics and optoelectronics.

We have then started studies for controlling the size and separation of the metal particles. Although our ultimate goal is to obtain the high-efficiency solid-state solar cells, we are presently studying n-Si PEC solar cells because they are convenient for testing how well the metal particles are deposited since they are made by simply immersing the n-Si electrode in the electrolyte solution. In the present work, we prepare Langmuir layers of Pt colloid particles for controlling the Pt particle distribution on n-Si wafers on a nanometer scale.

Recently some studies have been made on the preparation of fine particles on solid substrates by using the Langmuir-Blodgett (LB) layers, e. g., Fe_3O_4 (ca. 10nm) on Si or poly(ethylene terephthalate) [19], Fe_3O_4 (5 nm) on SiO_2/Si [20], CdS or ZnS (2.5 - 10 nm) on quartz or HOPG [21], CdS (5 nm) on glass [22], Pt on glassy carbon [23], though the size, and especially the separation of the fine particles on the substrates, were not well controlled.

Experimental

The Pt colloid solutions were prepared by the alcohol reduction method [16, 24]. 25 cm^3 of an aqueous solution of 1.32×10^{-3} M hexachloroplatinic(IV) acid was mixed with 25 cm^3 of an ethanol solution of 1.32×10^{-3} M (in monomer unit) poly(N-vinyl-2-pyrrolidone) (M.W. 40,000, this is hereafter abbreviated as PVP). The mixed solution was refluxed for 1 h by using an oil bath at the bath temperature of ca. 100°C. The color of the solution changed from yellow to dark brown. Stable and homogeneous Pt colloid solutions were obtained by this method, probably with PVP acting as a stabilizer.

The LB layers were prepared using a Langmuir trough made of Teflon, equipped with a Wilhelmy-type surface pressure measuring unit. The Pt colloid solution of 2 - 4 cm^3 was dropped and spread on a cleaned water surface of 803.5 cm^2 slowly at a rate of 0.05 cm^3/min with an automatic buret (Kyoto Electronics APB-118). After leaving the layer as it was for 10 min, it was compressed by moving a Teflon barrier and its area was reduced at a rate of 16.7 cm^2/min. The Langmuir layer of the Pt colloid particles thus prepared on a water surface was transferred onto an n-Si wafer by the horizontal lifting method.

Single crystal n-Si wafers [Shin-Etsu Handotai Co., Ltd., CZ, (100), ρ = 0.8 - 1.16 Ωcm, $N_D = (3 - 6) \times 10^{15}$ cm^{-3} as estimated from the ρ values [15], 0.42 mm thick] were cut into pieces 8 × 8 mm^2 in area and washed in boiling acetone for 2 min, then water rinsed. Just before transferring the Langmuir layer of the Pt particles, the n-Si wafers were immersed in a CP-4A solution [a mixture of water, hydrofluoric acid, nitric acid and acetic acid (22:3:5:3 in volume)] for 2 min, washed with water, etched with 12 % hydrofluoric acid for 2 min, and washed with water. After the

transferring of the LB layers of the Pt particles, the n-Si wafers were in most cases heat-treated at 200°C in a vacuum of 1.3×10^{-4} Pa for 30 min.

Ohmic contact was made with indium-gallium alloy on the rear surface of the n-Si wafer. It was fixed to a Teflon holder (0.25 cm^2 in effective area) [25] and used as an n-Si electrode for photoelectrochemical measurements. A large-area Pt plate was used as the counterelectrode, and a 8.6 M hydrogen bromide (HBr) and 0.05 M bromine (Br_2) aqueous solution was used as the redox solution. Photocurrent density vs. potential (j-U) curves were obtained with a potentiostat and a potential programmer, the potential of the n-Si electrode being measured with respect to the Pt counterelectrode. The n-Si electrode was irradiated with simulated solar AM1 (100 $mWcm^{-2}$) light using a solar simulator (Wacom WXS-85H). The solution was stirred magnetically during the j-U measurements.

Water was purified using a Milli-Q SP.TOC system (Japan Millipore Ltd.) with a 0.22 μm filter (Millipac-40) at the outlet. The resistivity of the water was more than 18 MΩcm. Reagent-grade chemicals (Ishizu Seiyaku and Tokyo Chemical Industry) were used without further purification.

The surface inspection was performed with scanning electron microscopes (Hitachi S-4100, S-5000), a transmission electron microscope (Hitachi H-9000), a non-contact atomic force microscope (NC-AFM, Seiko Instruments SPI3700), and a contact-mode atomic force microscope (AFM, Digital Instruments Nano Scope III). An energy dispersive X-ray spectroscopic (EDX) analysis was carried out with a Horiba EMAX-2770 spectrometer. An inductively coupled plasma (ICP) emission spectroscopic analysis was performed with a Perkin-Elmer ICP/5500 spectrometer.

Results

Solid lines in Fig. 1 show the surface pressure (π) vs. area per PVP molecule (A), obtained when the Pt colloid solution containing PVP as the stabilizer was developed on a clean water surface. The surface pressure gradually rose as the area per PVP molecule decreased, clearly indicating that a Langmuir-type layer of the Pt colloid particles is formed. The π-A curve is discontinuous at points marked by a, b and c in Fig. 1. This is due to the fact that the compression of the layer was stopped at these points (including point d) for about 15 min in order to transfer the Langmuir layer onto the n-Si wafers.

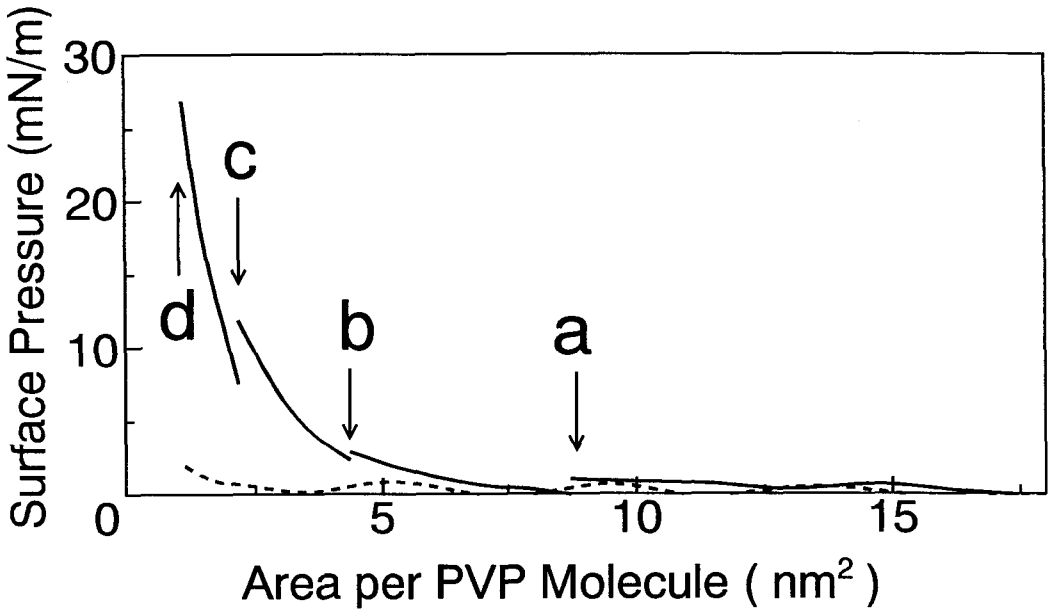

Figure 1. Surface pressure (π) vs. area per PVP molecule (A) (solid lines) obtained when the Pt colloid solution containing PVP was developed on a water surface at 18.5°C, and the same (dashed line) obtained when an ethanol solution of PVP was developed at 16.8°C.

The dashed line of Fig. 1 shows, for comparison, the π-A curve obtained when an ethanol solution of PVP containing no Pt particle was developed on a water surface and compressed. The surface pressure was very small, almost 0.0 mN/m, even at an area of 3 nm^2 per PVP molecule, because PVP is a water-soluble polymer. This result indicates that the π-A curve of the solid lines in Fig. 1 is truly due to the Langmuir layer of the Pt particles.

Figure 2 a, b and c show scanning electron micrographs (SEM) for n-Si wafers coated with the LB layer of the Pt particles. The micrographs a, b, and c are for the n-Si wafers on which the LB layer was transferred at the points a, b and c in the π-A curve of Fig. 1. Figure 2d is for the n-Si wafer on which the same Pt colloid solution was dropped and dried. White and black parts of the SEM's were confirmed to be Pt and Si, respectively, by the EDX analysis.

It is clearly seen from the SEM's that the Pt particles are fairly homogeneously distributed on the n-Si wafers with LB layers of the Pt colloid particles transferred, contrary to the case of dropping the Pt colloid solution and drying. Also, the density of the Pt particles increases with decreasing the area per PVP molecule, indicating that the separation of the Pt particles can be controlled by changing the area of the Langmuir layer.

Figure 3 shows a high resolution SEM of the same sample as Fig. 2b. Figure 4 exhibits a transmission electron micrograph (TEM) for the LB layer of the Pt colloid particles which was transferred onto a carbon-coated copper grid at A = 2.2 nm^2/PVP molecule. Black particles in the TEM were confirmed to be the Pt particles by the electron diffraction pattern. From Figs. 3 and 4, we can conclude that the Pt particles seen in Fig. 2 a, b and c, in general, consist of three-dimensional aggregates of several primary Pt particles, each being 2 to 6 nm in diameter.

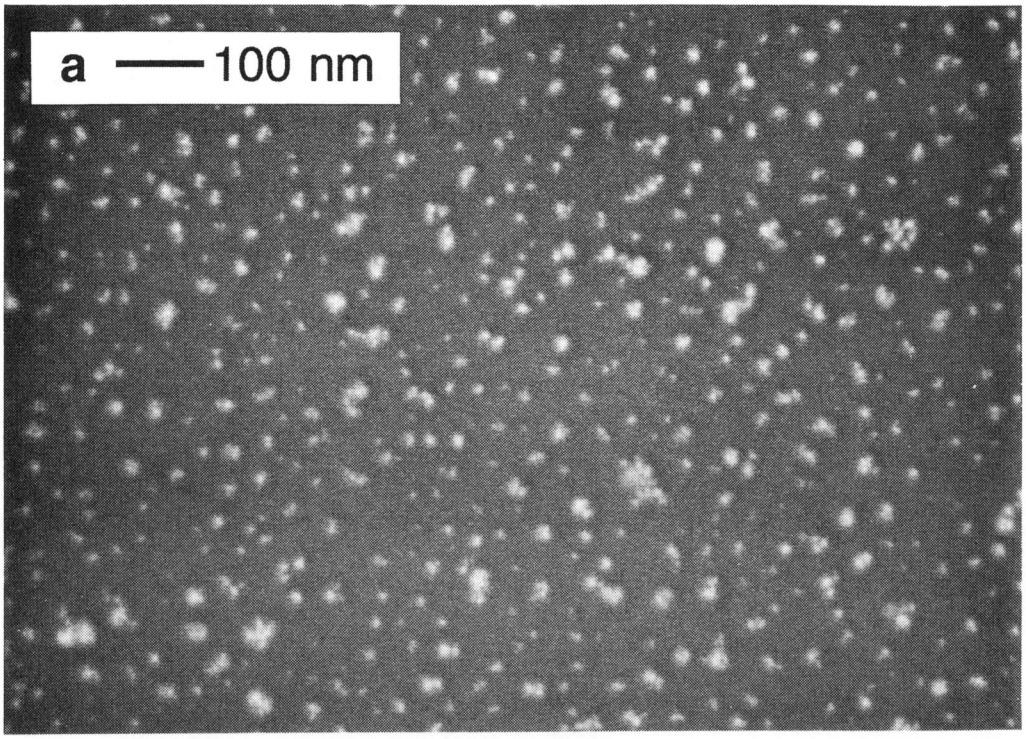
a —— 100 nm

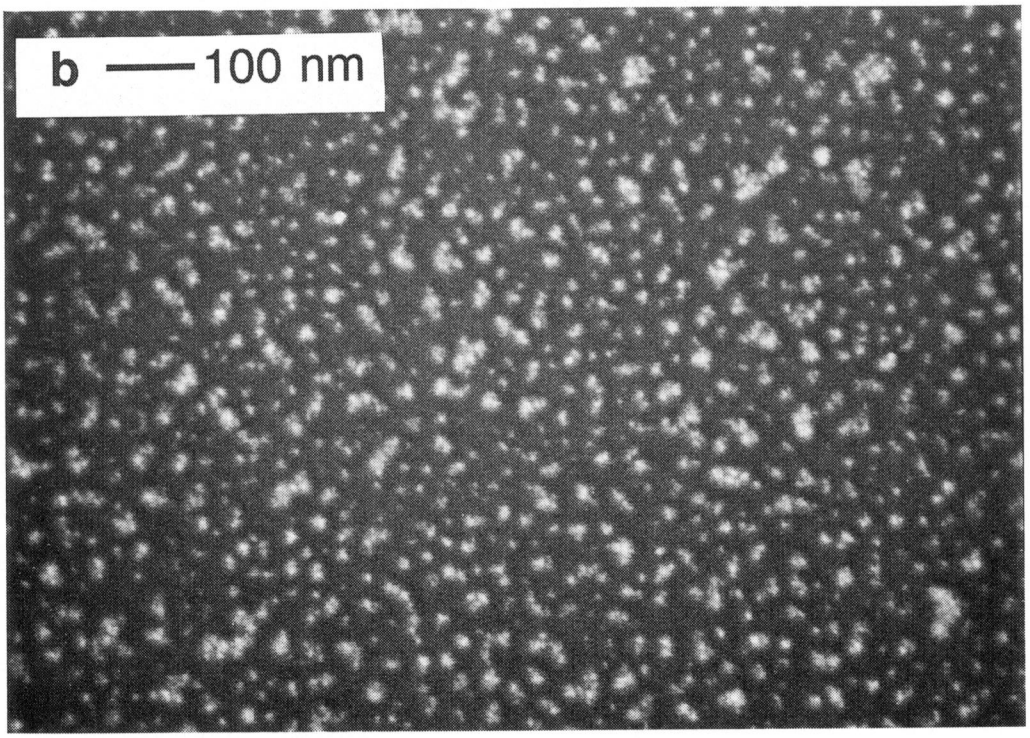
b —— 100 nm

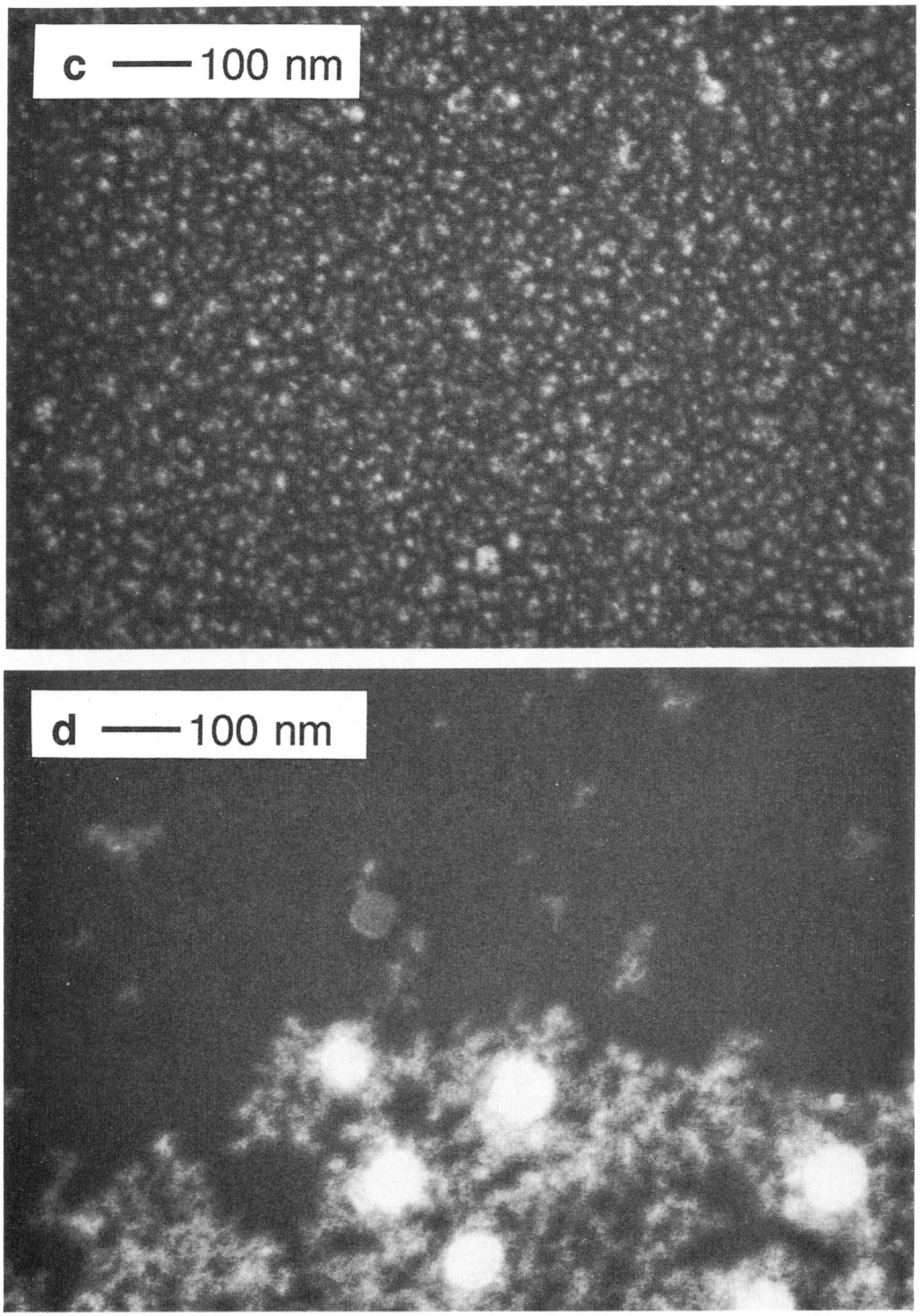

Figure 2. SEM's for the n-Si wafers coated with the LB layer of the Pt colloid particles. The marks a, b and c represent samples prepared by transferring the Langmuir layer at the points a, b and c in the π-A curve of Fig. 1. SEM (d) is for the n-Si wafer on which the Pt colloid solution was dropped and dried. The Pt-particle densities for a, b, c and d are 1.3, 2.7, 5.3 and 4.0 μgcm^{-2}.

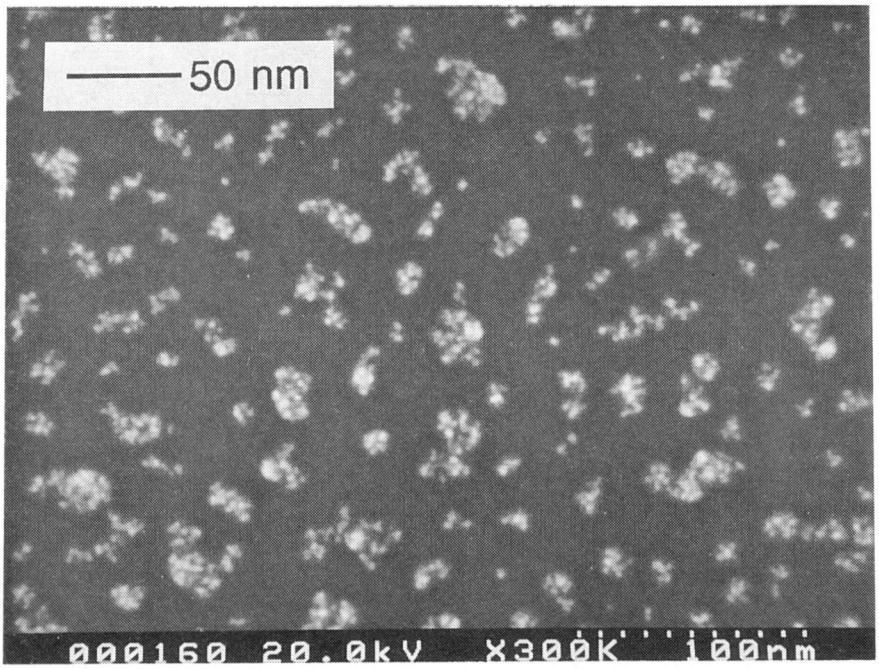

Figure 3. High-resolution SEM for the same sample as Fig. 2b.

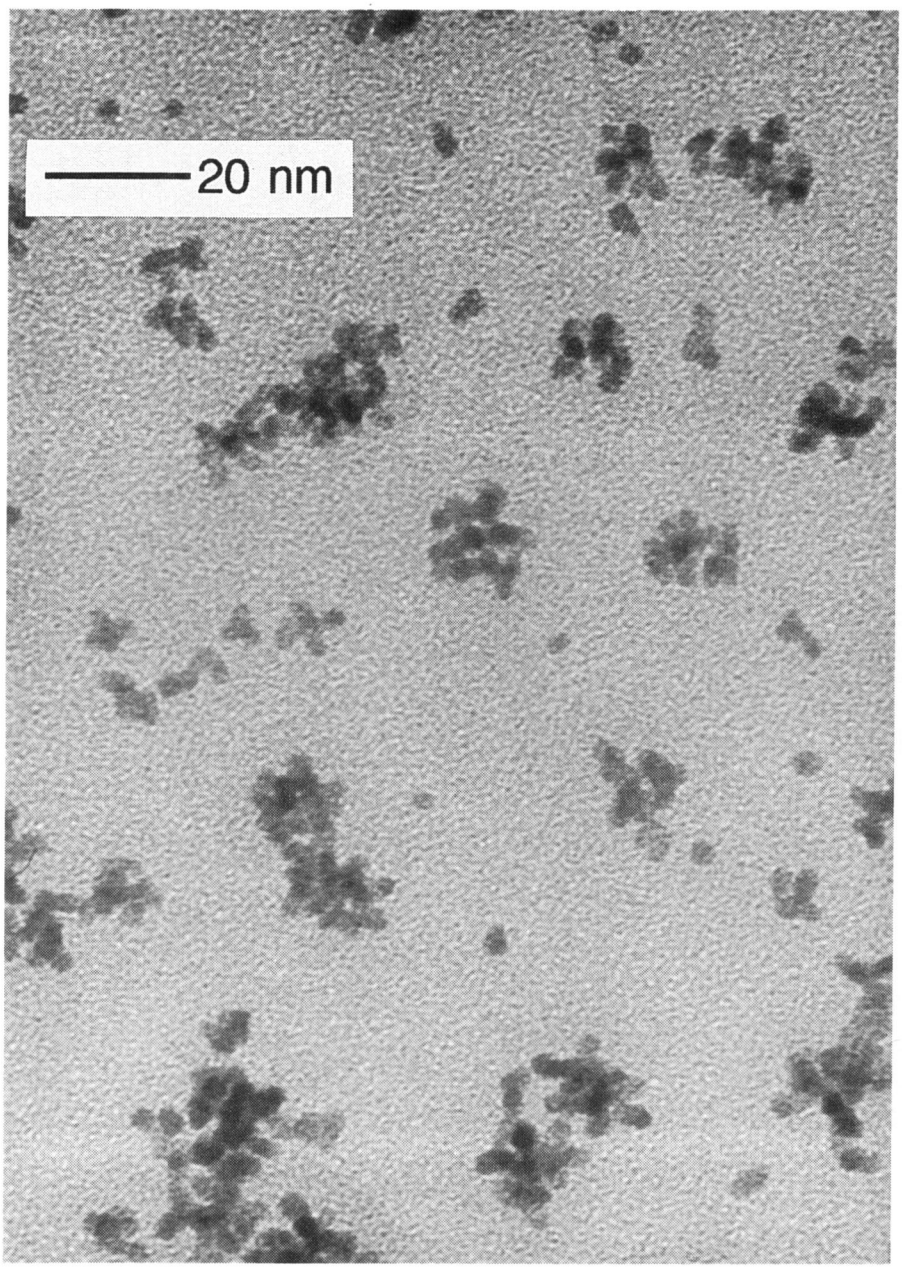

Figure 4. TEM for the LB layer of the Pt colloid particles transferred onto a carbon-coated copper grid. The Pt-particle density is 2.7 μgcm^{-2}.

Figure 5 shows a micrograph for the LB layer of the Pt colloid particles on n-Si when it was inspected by the non-contact atomic force microscopy (NC-AFM). The size of the primary Pt particles in the NC-AFM image is larger than that of the primary particles in the SEM and TEM. The inspection with the contact-mode atomic force microscopy (AFM) was also tried, but this method was not good for our samples because the Pt particles were moved by the tip of the microscope.

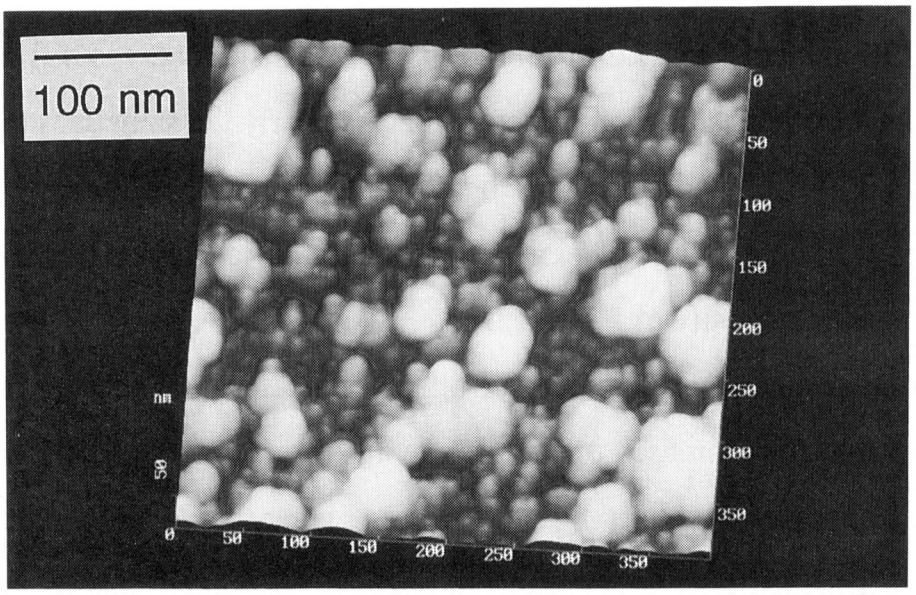

Figure 5. Non-contact AFM image for the n-Si wafer coated with the LB layer of the Pt colloid particles after the heat-treatment.

The Langmuir layers of the Pt colloid particles prepared by Bredig's method (50 nm in diameter) [16, 26] were also formed by developing an ethanol solution of the Pt colloid particles including oleic acid or sodium dodecylsulfate, on a water surface [11]. The density of the Pt particles on the n-Si wafer increased with decreasing the area of the Langmuir layer upon transferring it onto n-Si, similarly to the case of the PVP-stabilized Pt colloid.

The first to the fourth rows of Table 1 represent a typical example of the dependence on the Pt-particle density of solar cell characteristics for PEC cells, equipped with the n-Si electrodes modified with the LB layers of the Pt colloid particles. The Pt-particle density is expressed in a unit of μgcm^{-2} because it is difficult to estimate the number of Pt atoms in the Pt particles. The V_{OC} increases from 0.565 V to 0.610 V and the short-circuit photocurrent density (j_{SC}) also goes up from 23.7 $mAcm^{-2}$ to 27.2 $mAcm^{-2}$, as the Pt density decreases from 11 to 1.3 μgcm^{-2}. On the other hand, the fill factor (F.F.) is nearly the same in the Pt densities of 11 and 5.3 μgcm^{-2}, and decreases from 0.729 to 0.608 as the Pt density decreases from 5.3 to 1.3 μgcm^{-2}. The solar energy conversion efficiency (ϕ^S) has a maximum (11.3 %) at the Pt density of 5.3 μgcm^{-2}.

Similar results were obtained for other five series of experiments. It is to be noted here that the increases of the V_{OC} with decreasing the Pt density, such as mentioned above, were observed only in cases where all the n-Si electrodes with various Pt densities were prepared from one and the same Langmuir layer except that its area was changed. The n-Si electrodes prepared from different Langmuir layers gave different V_{OC}'s even though they had the same Pt density as calculated from the concentration and the dropped volume of the Pt colloid solution and the area of the Langmuir layer. In harmony with this result, the SEM inspection showed that the actual (absolute) densities of the Pt particles and the manner of their spatial

Table 1. Characteristics of PEC solar cells equipped with the n-Si electrode modified with the LB layer of the PVP-stabilized Pt-colloid particles, followed by heat-treatment at 200°C in vacuum for 30 min. The solution temperature was 25°C.

Pt density (μgcm^{-2})	V_{OC} (V)	j_{SC} ($mAcm^{-2}$)	F.F.	ϕ^S (%)
11	0.565	23.7	0.723	9.7
5.3	0.595	26.0	0.729	11.3
2.7	0.603	27.1	0.668	10.9
1.3	0.610	27.2	0.608	10.1
4.0[a)]	0.520[a)]	24.2[a)]	0.668[a)]	8.4[a)]

a) for the n-Si electrode on which the Pt colloid solution was simply dropped and dried, followed by the same heat-treatment as above.

distribution are different for the electrodes prepared from different Langmuir layers even if they had the same Pt density. The V_{OC} values obtained for the thirteen n-Si electrodes, each prepared from the different Langmuir layers at the (calculated) Pt density of 1.3 μgcm^{-2}, were in the range from 0.583 to 0.635 V at temperatures of 15 to 25°C, the average being 0.603 V.

The lowest row of Table 1 indicates the result for the n-Si electrode on which the Pt colloid solution was simply dropped and dried. The V_{OC} and ϕ^S are lower than those for the n-Si electrodes modified with the LB layer of the Pt particles shown in the upper rows.

All the solar-cell characteristics mentioned thus far are for the n-Si electrodes modified with the LB layers of the Pt particles and afterward heat-treated at 200°C in vacuum. If no heat-treatment was made, higher V_{OC}'s were obtained but the stability decreased. For example, the n-Si electrode modified with the 5.3 μgcm^{-2} Pt particles and not heat-treated gave a V_{OC} of 0.638 V at 17°C, but it decreased to 0.615 V after cyclic potential sweeping for 5 min. The F.F. also decreased from 0.649 to 0.583, though the j_{SC} of ~ 26 $mAcm^{-2}$ was kept unchanged.

The stability of the heat-treated electrodes was similar to that for the electrodes of the similar type reported in detail in Chapter 1. In order to examine whether the photoanodic dissolution of the Pt-particle modified n-Si electrode occurred or not, we also analyzed the electrolyte solution by ICP emission spectroscopy: The Si concentration of the 1.1 M HBr/0.026 M Br_2 solution (55.0 cm^3) was 2.25 - 2.27 ppm before the electrode illumination, and it changed to 2.29 - 2.37 ppm after continuous flow of the photocurrent to an amount of electricity of 813 C per 0.25 cm^2 (the area of the electrode surface). The increase of the Si concentration of 0.04 - 0.10 ppm is within the experimental errors, and is much smaller than the increase of 1.08×10^3 ppm expected for the case where all the photocurrent is assumed to correspond to the electrode dissolution.

Discussion

1) Preparation and structure of the LB layer of the ultrafine Pt particles

The π-A curve shown in Fig. 1 and the SEM's shown in Figs. 2 and 3 clearly show the Langmuir layer behavior. The Langmuir layer is schematically illustrated in Fig. 6. The Pt particles covered with PVP float on the water surface. PVP is water-soluble and thus PVP which is not adsorbed by the Pt particle is expected to be dissolved into the water phase.

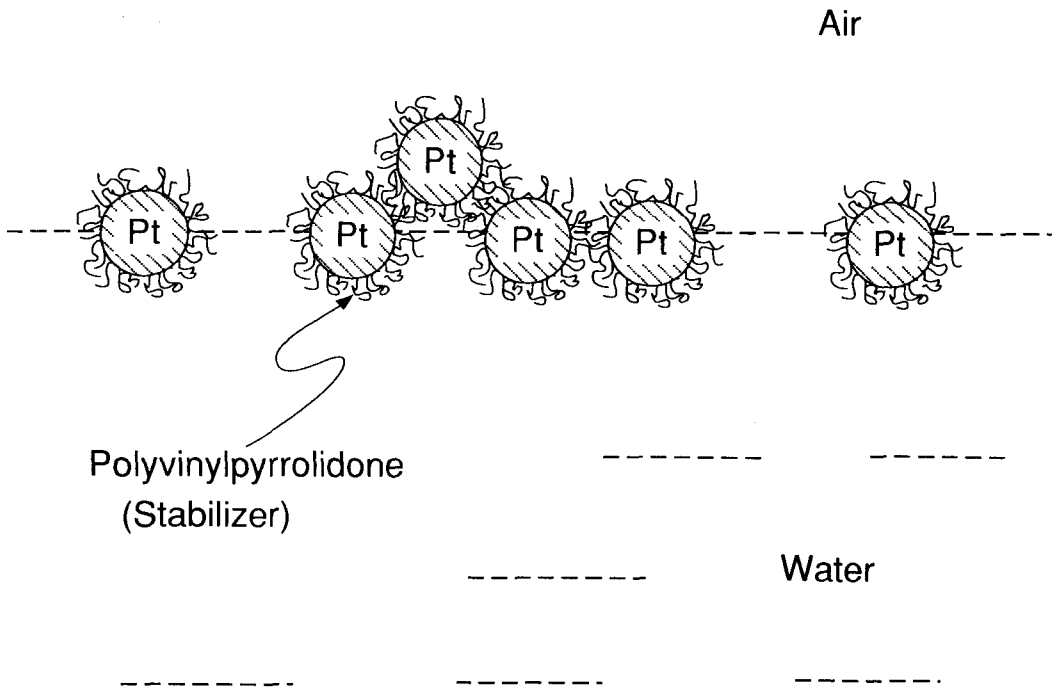

Figure 6. Schematic model of the Langmuir layer of the Pt colloid particles on a water surface.

The high-resolution SEM (Fig. 3) and NC-AFM image (Fig. 5) for the LB layer of the Pt particles on n-Si show that they aggregate three-dimensionally to some extent. It is not clear yet at which stage such aggregation occurs. However, most plausible is that the Pt particles aggregate already in the solution, because they aggregate even in the LB layer of the low Pt-particle density such as shown in Fig. 2a, and the extent of the aggregation is nearly independent of the Pt-particle density.

As mentioned before, the diameter of the Pt particles measured with the NC-AFM (Fig. 5) is larger than that measured with the SEM and TEM (Figs. 3 and 4). This is explained if we consider that the SEM and TEM represent the real size of the Pt particles, whereas the NC-AFM image exhibits the size of the PVP-covered Pt particles as a whole.

Figure 2 a, b, and c show that the Pt-particle density (or the separation of the Pt particles) can be controlled by changing the area of the Langmuir layer when it is transferred onto the n-Si wafer. Also, Toshima et al. reported [27] that the average size of colloidal metal particles prepared in the presence of PVP as the stabilizer could be changed in a range from 1.5 to 5.6 nm. The Pt colloid particles prepared by other methods such as Bredig's method [11, 16, 26] can also be used to make the LB layer, as mentioned in the preceding section. Accordingly, we can conclude that both the size and the separation of ultrafine metal particles on n-Si can be controlled on a nanometer scale by using the LB method.

2) Dependence of the solar cell characteristics on the Pt-particle density

The V_{OC} for the PEC cells equipped with the n-Si electrode modified with the Pt colloid particles increases with decreasing the Pt-particle density (Table 1). This is explained as follows: The V_{OC} for the solar cells is in general expressed by [11, 12, 28]

$$V_{OC} = (nkT/q) \ln(j_{SC}/j_0) \quad (1)$$

where n is the ideality factor, k the Boltzmann constant, T the temperature, q the elementary charge, j_{SC} the short-circuit photocurrent density, and j_0 the dark saturation current density. If recombination currents in the space charge layer and at the surface are neglected, j_0 is approximated by the sum of the majority and the minority carrier dark current densities, each expressed by j_{0n} and j_{0p}, respectively, and n = 1 holds.

As is seen from the SEM's in Figs. 2 and 3, the n-Si electrode used in the present work is sparsely coated with the very small Pt particles. The naked part of the n-Si surface should be covered with a thin Si oxide layer, as discussed in detail in Chapter 1. For the PEC cell equipped with such an n-Si electrode, the j_{0p} is given by [11,28]

$$j_{0p} = qD_pN_CN_V \exp(-E_g/kT) / L_pN_D \quad (2),$$

and is independent of the Pt-particle density and the Pt-particle size (or the effective potential barrier height in the n-Si). On the other hand, the j_{0n} is given by [11, 12]

$$j_{0n} = (S_{Pt}/S_0) A^*T^2 \exp(-q\phi_{eff}/kT) \quad (3)$$

where S_{Pt} refers to the area of the direct Pt-Si contact and S_0 the area of the whole Si surface, A^* is the modified Richardson constant, and ϕ_{eff} is the effective potential barrier height for the n-Si electrode coated with the Pt particles. Thus, the j_{0n} depends on the Pt-particle density and the Pt-particle size on n-Si because both S_{Pt} and ϕ_{eff} depend on them [12]. For the constant size of the Pt particles, as is the case in the present work, the decrease in the Pt-particle density lowers S_{Pt} and increases ϕ_{eff}, and hence reduces j_{0n}. Thus, the decrease in the Pt-particle density leads to the increase in V_{OC}. In an ultimate case where the Pt-particle density is very low, j_{0n} becomes much lower than j_{0p}, and the V_{OC} is mainly determined by j_{0p}. As the minority-carrier diffusion length (L_p) for the n-Si wafers ($N_D = (3 - 6) \times 10^{15}$ cm^{-3})

used in the present work was determined by an improved EBIC method reported by Ioannov et al. [29] to be 200 ± 5 μm, j_{0p} is calculated to be (0.68 - 1.4) × 10^{-8} Am^{-2} by using this value and values of D_p, N_C, N_V and E_g at 300 K reported in ref. 28. This j_{0p} value at 300 K gives V_{OC}'s of 0.63 - 0.64 V at 293 K (20°C), if the temperature dependence of j_{0p} is taken into account according to eq. (2) [30, 31], in harmony with the present experimental results.

The increase in j_{SC} with decreasing the Pt-particle density (Table 1) is explained easily as being due to the increase in the light intensity incident to the n-Si electrode. The decrease in the fill factor with decreasing the Pt-particle density is most probably caused by the increase of the photocurrent density at the surface of the Pt particles, which increases the overvoltage for the oxidation of bromide ions on Pt as well as increasing the ohmic drop at the Si-Pt contact.

The electrode stability is improved by the heat-treatment at 200°C in vacuum after transferring the LB layer of the Pt particles. This result can be explained on the basis of the model of the Langmuir layer of the Pt particles (Fig. 6) as follows: The Pt particles are covered with PVP and accordingly the PVP is present between the Pt particle and the n-Si surface for some of the Pt particles after the Langmuir layer was transferred onto the n-Si wafer. Such intervening PVP will prevent the Pt-Si direct contact or make it narrow and decrease the rate of hole transfer from n-Si to Pt. The heat-treatment will make PVP mobile and assist forming firm Pt-Si direct contact [16], thus leading to the stabilization of the electrode. It is to be noted here that the surface distribution of the Pt particles is not changed by the heat-treatment as confirmed by the SEM and the NC-AFM.

In conclusion, we have revealed in the present work that (1) a Langmuir layer of the ultrafine Pt particles can be formed on a water surface, (2) the size and the separation of the Pt particles on the n-Si electrode can be controlled on a nanometer

scale by use of the Langmuir layer, and (3) the characteristics for solar cells can be improved by controlling the Pt-particle density. The higher efficiency will be obtained if we can prevent aggregation of the Pt colloid particles, such as observed in Figs. 3 and 4.

References

1) A. M. Barnett, R. B. Hall, J. A. Rand, C. L. Kendall, and D. H. Ford, *Solar Energy Mater.*, **23**, 164 (1991).
2) T. L. Chu, S. S. Chu, and E. D. Stokes, *Solar Energy Mater.*, **2**, 265 (1979/1980).
3) M. Deguchi, H. Morikawa, T. Itagaki, T. Ishihara, and H. Namizaki, *Conf. Rec. IEEE Photovoltaic Spec. Conf.*, 22nd, 986 (1991).
4) T. Matsuyama, M. Tanaka, S. Tsuda, S. Nakano, and Y. Kuwano, *Jpn. J. Appl. Phys.*, **32**, 3720 (1993).
5) K. Ishii, H. Nishikawa, T. Takahashi, and Y. Hayashi, *Jpn. J. Appl. Phys.*, **32**, L770 (1993).
6) K. Zweibel and R. Mitchel, *Advances in Solar Energy*, Vol. 6, Edited by K. W. Böer, Ch. 5, American Solar Energy Soc., Inc. and Plenum Press, USA, (1990).
7) J. D. Levine, *AIP Conf. Proc.*, **268**, Photovoltaic Advanced Research & Development Project, Denver, CO, USA, 47 (1992).
8) J. F. Gibbons, G. W. Cogan, C. M. Gronet, and N. S. Lewis, *Appl. Phys. Lett.*, **45**, 1095 (1984).
9) G. Smestad, A. Ennaoui, S Fiechter, H. Tributsch, W. K. Hofmann, M. Birkholz, and W. Kautek, *Solar Energy Mater.*, **20**, 149 (1990).

10) B. O'Regan and M. Grätzel, *Nature*, **353**, 737 (1991).

11) Y. Nakato and H. Tsubomura, *Electrochim. Acta*, **37**, 897 (1992).

12) Y. Nakato, K. Ueda, H. Yano, and H. Tsubomura, *J. Phys. Chem.*, **92**, 2316 (1988).

13) Y. Nakato and H. Tsubomura, *Ber. Bunsenges. Phys. Chem.*, **91**, 405 (1987).

14) Y. Nakato, H. Yano, and H. Tsubomura, *Chem. Lett.*, 987 (1986).

15) K. Ueda, Y. Nakato, N. Suzuki, and H. Tsubomura, J. Electrochem. Soc., **136**, 2280 (1989).

16) S. Yae, R. Tsuda, T. Kai, K. Kikuchi, M. Uetsuji, T. Fujii, M. Fujitani, and Y. Nakato, *J. Electrochem. Soc.*, **141**, 3090 (1994).

17) Y. Nakato, H. Yano, S. Nishiura, T. Ueda, and H. Tsubomura, *J. Electroanal. Chem.*, **228**, 97 (1987).

18) Y. Nakato, S. Nishiura, H. Oshika, and H. Tsubomura, *Jpn. J. Appl. Phys.*, **28**, L261 (1989).

19) H. Kurio, K. Shibata, T. Nakaya, T. Matsuyama, H. Yamaoka, H. Tsuchiya, M. Okuno, and M. Imoto, *Polym. Prep., Jpn.*, **37**, 487 (1988).

20) X. K. Zhao, S. Xu, and J. H. Fendler, *J. Phys. Chem.*, **94**, 2573 (1990).

21) X. K. Zhao, Y. Yuan, and J. H. Fendler, *J. Chem. Soc., Chem. Commun.*, 1248 (1990).

22) E. S. Smotkin, C. Lee, A. J. Bard, A. Campion, M. A. Fox, T. E. Mallouk, S. E. Webber, and J. M. White, *Chem. Phys. Lett.*, **152**, 265 (1988).

23) M. Fujihira and S. Poosittisak, *Chem. Lett.*, 251 (1986).

24) H. Hirai, Y. Nakao, and N. Toshima, *J. Macromol. Sci.-Chem.*, **A12**, 1117 (1978), and **A13**, 727 (1979).

25) K. Ueda, Y. Nakato, and H. Tsubomura, *Solar Energy Mater.*, **17**, 37 (1988).

26) G. Bredig, Z. Angew. Chem., **11**, 951 (1898).

27) H. Hirai, H. Chawanya, and N. Toshima, *Reactive Polymers*, **3**, 127 (1985); N. Toshima, M. Harada, T. Yonezawa, K. Kushihashi, and K. Asakura, *J. Phys. Chem.*, **95**, 7448 (1991).

28) S. M. Sze, *Physics of Semiconductor Devices*, 2nd ed., Wiley, New York, (1981).

29) D. E. Ioannou and C. A. Dimitriadis, *IEEE Trans. Electron Devices*, **ED-29**, 445 (1982).

30) N. G. Tarr and D. L. Pulfrey, *Appl. Phys. Lett.*, **34**, 295 (1979).

31) H. Kobayashi, A. Chigami, N. Takeda, and H. Tsubomura, *J. Electroanal. Chem.*, **287**, 239 (1990).

Chapter 3

Minority Carrier Controlled PEC Solar Cells, Using n-Si Electrodes Modified with LB Layers of Ultrafine Pt Particles

Introduction

The main difficulty in recent solar-cell studies lies in how to reduce the production cost without lowering the conversion efficiency. Many attempts have been made from various aspects, using low-cost semiconductor materials [1-5] and/or low-cost junction-formation methods [5-9].

We have been studying silicon (Si) solar cells of a new type [10-16], in which n-Si wafers are modified sparsely with ultrafine metal particles, the naked part of the n-Si surface being covered with an insulating silicon oxide layer and passivated. The metal particles on n-Si act as minute channels for steady photocurrents, otherwise the whole Si surface is covered with the insulating silicon oxide layer and no photocurrent flows. The photoelectrochemical (PEC) solar cells of this type generate open-circuit photovoltages (V_{OC}'s) of 0.62 to 0.68 V [10-14], considerably higher than those for the conventional p-n junction Si solar cells of similar simple cell structure (0.59 V), clearly indicating the strong advantage of this-type solar cells. This method can be applied to low-cost semiconductor materials such as polycrystalline Si thin films. This method can also be extended to solid-state solar cells [10, 15, 16].

For obtaining high efficiencies and reproducible results in the above-type solar cells, it is important to deposit the metal particles with the size and the separation well-controlled on a nanometer scale [10, 11]. In Chapter 2, we have reported that the use of Langmuir-Blodgett (LB) layers of colloidal platinum (Pt) particles enables us to control their spatial distribution on n-Si on a nanometer scale. In this chapter we will report results of detailed studies on such n-Si electrodes, with a focus being placed on the effect of the Pt-particle density and the post-heat-treatment temperature on V_{OC}. The post-heat-treatment is made to obtain good electrical contact between polymer-stabilized Pt particles and n-Si.

Experimental

Pt colloid solutions were prepared by reducing hexachloroplatinic(IV) acid with ethanol in the presence of poly(N-vinyl-2-pyrrolidone) (M.W. 40,000) as reported in Chapter 2. The diameter of the Pt-particles obtained was 2-6 nm as determined with a Hitachi H-9000 transmission electron microscope.

The Langmuir layers of the Pt colloid particles were developed on a water surface also as reported in Chapter 2. The layer was transferred onto an n-Si wafer by the horizontal lifting method.

Single crystal n-Si wafers [Shin-Etsu Handotai Co., Ltd., CZ, (100), 0.8 - 1.16 Ωcm, 0.42 mm thick] were cut into pieces 8 × 8 mm^2 in area, washed with boiling acetone for 2 min, and rinsed with water. Just before transferring the Langmuir layer of the Pt particles, the n-Si wafers were etched with CP-4A [a mixture of water, hydrofluoric acid, nitric acid and acetic acid (22:3:5:3 in volume)] and 12 % hydrofluoric acid. After the transfer of the Langmuir layers, the n-Si wafers were

in most cases heat-treated at a temperature from 150 to 300 ° C in a vacuum of 1.3 $\times 10^{-4}$ Pa for 30 min.

Photocurrent density vs. potential (j-U) curves were obtained with a potentiostat and a potential programmer. A large-area Pt plate was used as the counterelectrode, and a 8.6 mol/dm^3 hydrogen bromide and 0.05 mol/dm^3 bromine aqueous solution was used as the redox electrolyte. The electrode illumination was normally performed by simulated solar AM1.5G (100 mW/cm^2) light using a Wacom WXS-85H solar simulator. For measurements of short-circuit photocurrent densities (j_{SC}) vs. V_{OC}, a tungsten-halogen lamp was used as the light source. The solution was stirred magnetically, and temperature changes of the electrolyte solution were kept less than 2° C during the measurements. Further experimental details are reported in Chapter 2.

Results

Figure 1 shows V_{OC}'s for the PEC solar cells equipped with the n-Si electrodes modified with the LB layer of the Pt particles as a function of the Pt-particle density. The V_{OC}'s were determined from measurements of the photocurrent (j) - potential (U) curves. Plot a is for the electrodes with no post-heat-treatment after the Pt deposition. The j-U curves in this case were not so stable, gradually changing with time during cyclic potential scans, and the V_{OC}'s were determined from the j-U curves in the first scan. Plots b, c and d are for the electrodes which were heat-treated at 150, 200 and 300 ° C respectively after the Pt deposition. Such heat-treated electrodes were stable during potential scans for 60 min.

It is first noticed that the V_{OC}'s for the electrodes with no heat-treatment and the electrodes with the heat-treatment at 150°C are in the range of 0.61 to 0.63 V, independent of the Pt-particle density (plots a and b in Fig. 1). On the other hand, the V_{OC}'s for the electrodes with the heat-treatments at 200 and 300 ° C increase with the decrease in the Pt-particle density. A similar result was already reported for the electrodes heat-treated at 200 ° C in Chapter 2.

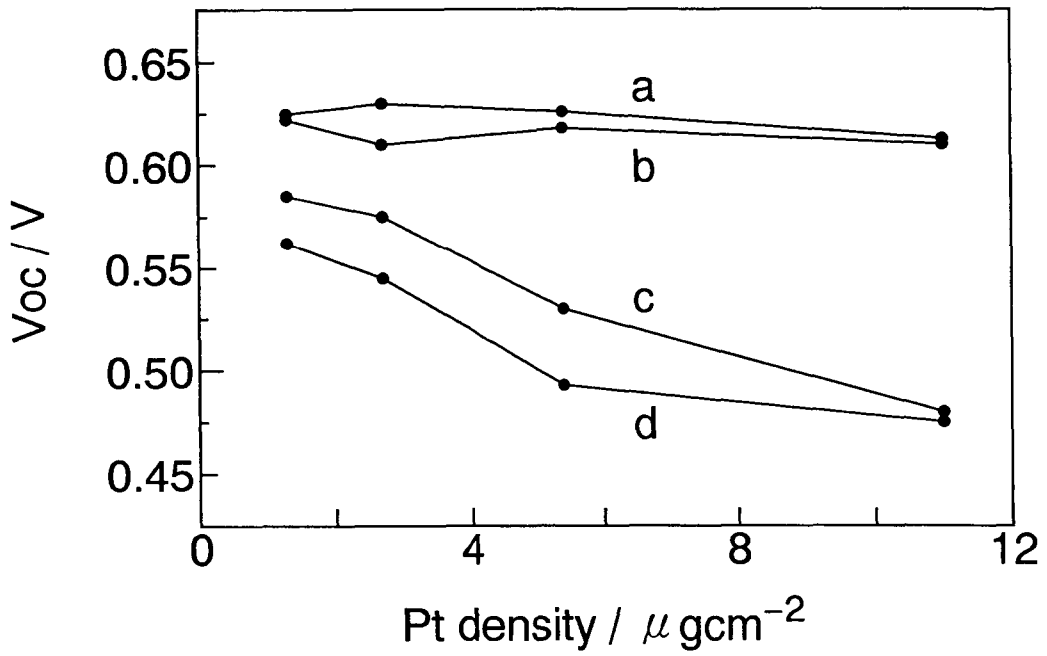

Figure 1. Open-circuit photovoltages (V_{OC}) vs. the Pt-particle density for the n-Si electrodes modified with the Pt particles: a is for the electrodes just modified with Pt and not heat-treated, and b, c and d are for the electrodes heat-treated at 150, 200 and 300 °C respectively after the Pt modification. The solution temperature in the PEC solar cells was 17-25 °C.

The V_{OC} for solar cells is in general given by [17]

$$V_{OC} = (nkT/q) \ln (j_{SC}/j_0) \quad (1)$$

where n is the ideality factor, q the elementary charge, j_{SC} the short-circuit photocurrent density, and j_0 the dark saturation current density. Accordingly, n and j_0 can be obtained from ln j_{SC} vs. V_{OC} plots. Figure 2 shows such plots for the n-Si electrodes modified with the LB layers of the Pt particles and heat-treated at 200° C. The V_{OC} and j_{SC} were changed by changing the illumination intensity. Good straight lines are obtained, and the n and j_0 values determined from the plots are listed in Table 1. The n is accurately unity, independent of the Pt density. However, the j_0 increases and hence the V_{OC} decreases with increasing the Pt density.

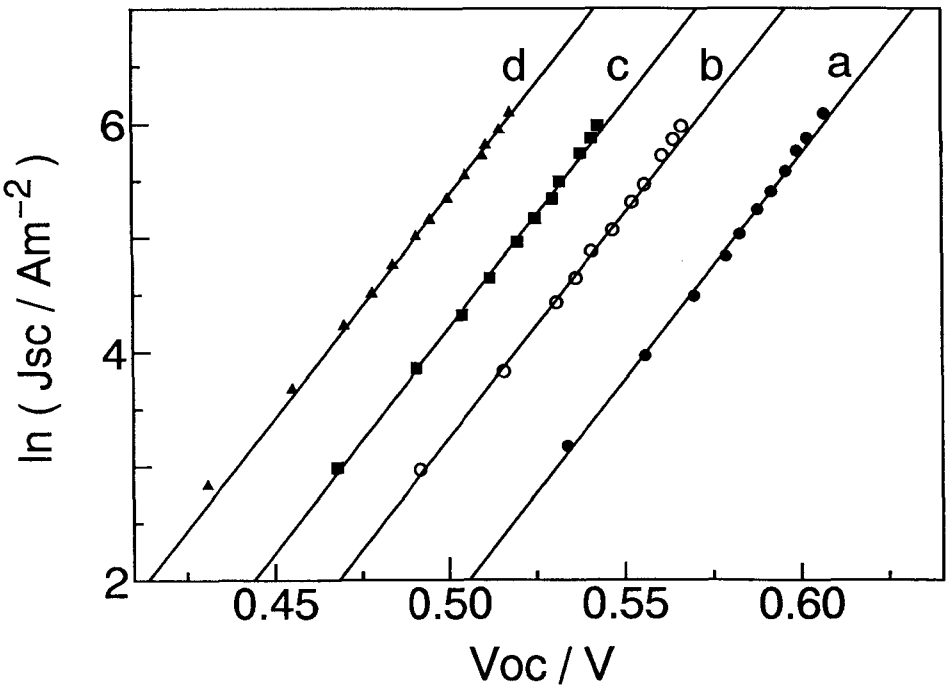

Figure 2. Plots of ln j_{SC} vs. V_{OC} for the n-Si electrodes modified with the Pt particles and heat-treated at 200 °C: a, b, c and d are for the electrodes modified at the Pt density of 1.3, 2.7, 5.3 and 11 μgcm^{-2}, respectively.

Table 2 shows the effect of the post-heat-treatment temperature on the n and j_0 values for the n-Si electrodes having the Pt density of 1.3 $\mu g/cm^2$ (see footnote a of Table 1). The n is again accurately unity, independent of the heat-treatment temperature. The j_0 increases and the V_{OC} decreases with increasing the heat-treatment temperature.

Table 3 shows, for reference, the n and j_0 values obtained for the n-Si electrodes modified with Pt-colloid particles (14 - 50 nm in diameter) prepared by Bredig's method [14]. The Pt particles in this case were deposited by the method of dropping a Pt colloid solution and drying. The first row of Table 3 is for the n-Si electrode with no heat-treatment. The second and the third rows are for the n-Si electrodes with heat-treatments at 300 ° C for 10 min in vacuum after the deposition of the Pt particles, though the electrode in the third row is slightly oxidized at the surface by immersing in 63 % nitric acid for 10 min at room temperature before dropping the Pt colloid solution. The V_{OC} and the j_{SC} values for these electrodes were reported in Chapter 1. The n is nearly unity for all the cases, but the j_0 changes with the electrode preparation conditions. The slight pre-oxidation of the n-Si surface reduced the j_0 as can be seen from comparison of the second and third rows.

Discussion

For the present-type solar cells equipped with the Pt-modified n-Si electrodes, the ideality factor n is accurately (or nearly) unity, independent of the Pt-particle density and the heat-treatment temperature (Tables 1~3). This result indicates that almost no electron-hole recombination occurs at the electrode surface as well as in

Table 1. The ideality factor (n) and the dark saturation current density (j_0) for the n-Si electrodes modified with the Pt particles and heat-treated at 200 °C. The solution temperature in the PEC solar cells was 24 ± 1 °C.

Pt density[a] (μgcm^{-2})	n	j_0 (10^{-7} Am^{-2})	V_{OC} (exp)[b] (V)	V_{OC} (calc)[c] (V)
1.3	0.99	0.16	0.596	0.595
2.7	1.00	0.82	0.556	0.558
5.3	0.99	1.9	0.532	0.533
11	1.00	7.3	0.505	0.504

a) This Pt density was calculated by assuming that all the Pt particles in a Pt colloid solution dropped on a water surface formed a Langmuir layer and that it was transferred completely onto the n-Si electrode.

b) Values observed when $j_{SC} = 25$ $mAcm^{-2}$.

c) Values calculated from Eq. 1 by using the n and j_0 values listed above and taking $j_{SC} = 25$ $mAcm^{-2}$.

Table 2. The n and j_0 values for the n-Si electrodes modified with the 1.3 μgcm^{-2} Pt particles and heat-treated at various temperatures. The solution temperature was 21 ± 1 °C.

Heat-treatment temperature (°C)	n	j_0 (10^{-7} Am^{-2})	j_{SC} (exp) ($mAcm^{-2}$)	V_{OC} (exp) (V)	V_{OC} (calc)[a] (V)
150	1.01	0.093	22.2	0.610	0.610
200	1.01	0.36	22.4	0.585	0.575
300	1.00	1.1	21.5	0.555	0.542

a) Values calculated from Eq. 1 using the n, j_0 and j_{SC}(exp) values listed above.

Table 3. The n and j_0 values for the n-Si electrodes modified with the Bredig's method Pt colloid particles. The solution temperature was 24 ± 1 °C.

Electrode treatment[a]	n	j_0 (10^{-7} Am^{-2})	j_{SC} (exp) ($mAcm^{-2}$)	V_{OC} (exp) (V)	V_{OC} (calc)[b] (V)
not heat-treated	1.01	0.103	27.9	0.603	0.609
heat-treated	1.03	7.9	24.7	0.515	0.518
pre-oxidized and heat-treated	1.02	0.39	25.5	0.575	0.575

a) See text for details.

b) V_{OC} calculated from Eq. 1 using the n, j_0 and j_{SC}(exp) values listed above.

the space charge layer of the n-Si electrode, implying that an ideal n-Si/solution junction is formed. The Pt particles in the present work are very small and sparsely scattered on the n-Si electrode [13], and therefore the major part of its surface is covered with a thin Si oxide layer and passivated, where the density of interface states (recombination centers) are very low [14]. Also, the Pt particles are softly deposited on the n-Si, so as not to form any defects at the surface and in the space charge layer. These seem to result in the formation of such an ideal junction.

Since n is unity as mentioned above, it follows that the change of the dark saturation current density j_0 is the only reason for the V_{OC} change. We first consider the decrease of V_{OC} by the increase in the Pt density for the n-Si electrodes with heat-treatments at 200 or 300°C (Fig. 1, plot c and d, and Table 1). As n is unity, j_0 can be expressed by the sum of the majority and the minority carrier dark current densities, each expressed by j_{0n} and j_{0p}, respectively, i.e., $j_0 = j_{0n} + j_{0p}$. For the present n-Si electrode modified with the Pt particles, j_{0p} is given by [10, 17]

$$j_{0p} = qD_pN_CN_V \exp(-E_g/kT) / L_pN_D \qquad (2),$$

and is independent of both the Pt-particle density on the n-Si surface and the effective barrier height (ϕ_{eff}) for the electrode. On the other hand, j_{0n} is given by [10, 11]

$$j_{0n} = (S_{Pt}/S_0) A^*T^2 \exp(-q\phi_{eff}/kT) \qquad (3)$$

where S_{Pt} refers to the area of the direct Pt-Si contacts and S_0 does the area of the whole Si surface. A^* is the modified Richardson constant. It is assumed in Eq. 3 that the conduction band electrons can flow into the redox solution only though the Pt particles. Thus, j_{0n} increases with increasing the Pt density or S_{Pt}/S_0. The j_{0n} also depends on ϕ_{eff}. The increase in the width of the direct Pt-Si contacts lowers ϕ_{eff} [10, 11], and the decrease in ϕ_{eff} increases j_{0n}. Accordingly, the above-mentioned

decrease of V_{OC} with the increase in the Pt density can attributed to the increase in S_{Pt}/S_0 and the decrease in ϕ_{eff}.

Next we consider the effect of the heat-treatment temperature on V_{OC}. With the high Pt density, the V_{OC} decreases as the heat-treatment temperature increases (Fig. 1 and Table 2). Also, for the low heat-treatment temperature of 150°C or no heat-treatment, V_{OC} is nearly independent of the Pt density (Fig. 1). These results can be explained as follows.

In the present work, the Pt particles are covered with polyvinylpyrrolidone (PVP) acting as a stabilizer and thus PVP is present between the Pt particle and the n-Si surface. Such intervening PVP prevents the Pt-Si direct contact or makes its area narrow. However, the heat-treatments of the n-Si wafers will make PVP mobile and increase the number and the area of the Pt-Si direct contacts. Thus, the increase in the heat-treatment temperature, in general, increases S_{Pt} and lowers ϕ_{eff}, and then increases j_{0n}, resulting in the decrease in V_{OC}. SEM inspection before and after the heat-treatments showed that the spatial distribution of the Pt particles on the n-Si surface was not changed by the heat-treatments.

Based on the above argument, the constant and high V_{OC} values for the n-Si electrodes with no heat-treatment or with the heat-treatment at the low temperature of 150°C (Fig. 1), independent of the Pt density, can be explained by assuming that the Pt-Si direct contacts are small in number and narrow in these cases and $j_{0n} \leq j_{0p}$ holds. From internal quantum efficiency measurements, the minority-carrier diffusion length (L_p) for the Pt-particle modified n-Si electrodes was determined to be in the range of 180 to 240 μm [18]. From this value, the j_{0p} is calculated, using Eq. 2, to be (0.57-1.5) × 10^{-8} Am^{-2} at 300 K [17], or (0.22-0.58) × 10^{-8} Am^{-2} at 294 K by taking account of the temperature dependences of D_p, N_C, N_V, E_g and L_p [19-21]. This j_{0p} value at 294 K is of the same order of magnitude as the observed

j_0 ($= j_{0n} + j_{0p}$) value (0.93×10^{-8} Am^{-2}) for the n-Si electrodes modified with the 1.3 μgcm^{-2} Pt particle and heat-treated at 150°C (the first row of Table 2). This indicates that $j_{0n} \leq j_{0p}$ holds within the experimental errors. Also, for the electrodes not heat-treated and heat-treated at 150°C, the V_{OC} is nearly independent of the Pt density and ranges from 0.61 to 0.63 V, as mentioned before. This fact also implies that $j_{0n} \leq j_{0p}$. If we assume that $j_0 = j_{0p}$ and $j_{0n} \approx 0$, V_{OC} is calculated from Eq. 1 and the above j_{0p} values to be in the range of 0.61 to 0.65 V for j_{SC} of 25 $mAcm^{-2}$, in good agreement with the observed values. From these considerations, we can conclude that $j_{0n} \leq j_{0p}$ holds for the n-Si electrodes heat-treated at 150°C or not heat-treated, V_{OC} being mainly determined by the minority carrier dark current j_{0p}.

In conclusion, we have revealed that (*i*) the ideality factor n is unity for all the n-Si electrodes modified with the ultrafine Pt particles, indicative of that an ideal n-Si/solution junction is formed, and (*ii*) the majority carrier dark current density (j_{0n}) can be decreased very much by decreasing the Pt-particle density and the post-heat-treatment temperature, and minority carrier controlled diodes (solar cells) can be obtained under appropriate conditions. The electrode stability in the present PEC solar cells is not enough for practical application, but this problem can be solved if the solid-state solar cells of the same type are developed as discussed in our previous papers [13, 14, 16]. The present results are useful to develop such efficient solid-state solar cells.

References

1) A. M. Barnett, R. B. Hall, J. A. Rand, C. L. Kendall, and D. H. Ford, *Solar Energy Mater.*, **23**, 164 (1991).

2) S. Arimoto, H. Morikawa, M. Deguchi, Y. Kawama, Y. Matsuno, T. Ishihara, H. Kumabe, and T. Murotani, *Sol. Energy Mater. Sol. Cells*, **34**, 257 (1994).

3) J. D. Levine, *AIP Conf.*, **268** (Photovoltaic Advanced Research & Development Project, Denver, CO), p. 47 (1992).

4) K. Zweibel and R. Mitchel, *Advances in Solar Energy*, Vol. 6, Edited by K. W. Böer, Ch. 5, American Solar Energy Soc., Inc. and Plenum Press (1990).

5) *Phys. Chem. Mater. Low-Dimens. Struct.*, **14** (Photoelectrochem. Photovoltaics of Layered Semicond.), Edited by A. Aruchamy, Kluwer Academic Publishers, Netherlands (1992).

6) R. Memming, *Topics in Current Chemistry*, **143**, 79 (1988).

7) B. Miller, S. L. Licht, M. E. Orazem, and P. C. Searson, *Crit. Rev. Surf. Chem.*, **3**, 29 (1993).

8) K. S. Chandra Babu, O. N. Srivastava, and G. V. Subba Rao, *Curr. Sci.*, **66**, 715 (1994).

9) H. Kobayashi, Y. Kogetsu, T. Ishida, and Y. Nakato, *J. Appl. Phys.*, **74**, 4756 (1993).

10) Y. Nakato and H. Tsubomura, *Electrochim. Acta*, **37**, 897 (1992).

11) Y. Nakato, K. Ueda, H. Yano, and H. Tsubomura, *J. Phys. Chem.*, **92**, 2316 (1988).

12) K. Ueda, Y. Nakato, N. Suzuki, and H. Tsubomura, *J. Electrochem. Soc.*, **136**, 2280 (1989).

13) S. Yae, I. Nakanishi, Y. Nakato, N. Toshima, and H. Mori, *J. Electrochem. Soc.*, **141**, 3077 (1994).

14) S. Yae, R. Tsuda, T. Kai, K. Kikuchi, M. Uetsuji, T. Fujii, M. Fujitani, and Y. Nakato, *J. Electrochem. Soc.*, **141**, 3090

15) Y. Nakato, S. Nishiura, H. Oshika, and H. Tsubomura, *Jpn. J. Appl. Phys.*, **28**, L261 (1989).

16) Y. Nakato, K. Kai, and K. Kawabe, *Sol. Energy Mater. Sol. Cells*, **37**, 323 (1995).

17) S. M. Sze, *Physics of Semiconductor Devices*, 2nd ed., John Wiley & Sons, New York (1981).

18) J. G. Jia, M. Fujitani, S. Yae, and Y. Nakato, *Electrochim. Acta,* **42**, 431 (1996).

19) N. G. Tarr and D. L. Pulfrey, *Appl. Phys. Lett.*, **34**, 295 (1979).

20) H. Kobayashi, A. Chigami, N. Takeda, and H. Tsubomura, *J. Electroanal. Chem.*, **287**, 239 (1990).

21) *Properties of Silicon*, EMIS Datareviews Series No.4, INSPEC, The Institution of Electrical Engineers, London and New York (1987).

Chapter 4

Improvement in Photovoltage and Stability of Porous n-Si Electrodes Coated with Platinum by Regulation of the Thickness of Nanoporous Layers

Introduction

Porous silicon (Si) has recently attracted much attention as a promising material for light emitting diodes (LED's) because it exhibits photo- and electroluminescences efficiently in the visible region [1-5]. Solar cells are closely related with LED's, operating by a reverse mechanism to each other with respect to conversion between light and electric energies. For achieving high performances in such devices, it is important to clarify the structure and properties of porous Si layers and find a way to control them.

Considerable studies have been made on solar cells using porous Si. For p-n junction based solid-state solar cells [6-10], porous Si is used mainly for decrease in the surface light reflectance and increase in the photocurrent density. For photoelectrochemical (PEC) solar cells [11-17], the situation is rather complicated, a variety of photocurrents, photovoltages and stability being reported probably because of differences in the detailed structure of porous (or nanoporous) Si layers. Some beneficial effects of using porous Si on the photovoltage were reported for hydrogen evolution on Pt-deposited p-Si [11], photooxidation reaction on n-Si in 57% HI [13, 14], and photoreduction reaction on p-Si in nonaqueous electrolyte

containing a cobaltocene/cobaltocinium redox couple [15], and the role of porous Si in suppressing surface recombination and stabilizing the Si electrode was discussed [14, 15].

We reported before [16] that the V_{OC} for Pt-coated n-Si electrode was increased by making a porous Si layer and explained the result by a new effect of nanometer-sized Pt-dot contacts. The purpose of the present paper is to investigate in detail the structure and properties of the Pt-coated porous n-Si electrodes on the basis of our recent advanced knowledge on the porous Si layers and the metal-dot contacts [17-20] and to search for factors to improve the characteristics.

Experimental

Single crystal n-Si wafers (Shin-Etsu Handotai Co., Ltd., CZ, <100>, 0.95-1.05 Ωcm) were cut into pieces 1 × 1 cm^2 in area, washed with boiling acetone and water, etched with CP-4A (a mixture of hydrofluoric acid, nitric acid, acetic acid and water (3:5:3:22 in volume)) and 12 % HF. Ohmic contacts were made on the rear side with indium-gallium alloy. The n-Si piece was then placed in a Teflon holder (effective area: 0.5 cm^2) and used as an n-Si electrode for the formation of a porous Si layer.

The porous Si layer was formed as follows: The n-Si electrode was illuminated (and etched) under an anodic bias in a mixture of water, 50% HF and ethanol (21:3:4 in volume) or a mixture of 50% HF and ethanol (6:1 in volume) . The n-Si surface was kept horizontal, with the etching cell placed in an ultrasonic bath (38 kHz), so that gas bubbles formed on the Si surface during the etching could easily be removed. The temperature of the cell solution was kept constant within ± 1 °C

using a temperature controller. A 300 W tungsten-halogen lamp was used as the light source. Currents vs. potential were measured with a commercial potentiostat/galvanostat and potential programmer. After stop of photoetching, the n-Si electrodes were in many cases kept in the above mentioned water-HF-ethanol solution at the same temperature as in the photoetching for 10 to 300 s without ultrasonic agitation in order to decrease the amount of the nanoporous layers.

Platinum was deposited on the n-Si wafer thus treated by the electron-beam evaporation method. The n-Si surface was inclined to the direction of the Pt vapor such that its incident angle was 75°. The Pt thickness was monitored with a quartz-oscillator placed perpendicular to the direction of the Pt vapor and regulated to be 7.0 nm as measured with this oscillator.

The Pt deposited porous n-Si wafer was again fixed to a Teflon holder and used for measurements of solar cell characteristics. A large-area Pt plate was used as the counterelectrode, and a 8.6 M hydrogen bromide (HBr) and 0.05 M bromine (Br_2) aqueous solution was used as the redox electrolyte. The n-Si electrode was irradiated with simulated solar AM 1.5G (100 $mWcm^{-2}$) light using a solar simulator (Wacom WXS-85H). The redox solution was stirred magnetically and kept at a temperature of 25 ± 1 °C during measurements.

The photoluminescence of porous n-Si layers was measured with a fluorescence spectrophotometer (Hitachi F4500). The structure of the porous layers was inspected with a high-resolution scanning electron microscope (Hitachi S-5000). Energy dispersive X-ray spectroscopic (EDX) analysis was carried out with a Horiba EMAX-2770 spectrometer. Photocurrent action spectra were obtained using a monochromator (Jobin Yvon H20) and a 300 W Xe-lamp. The intensity of monochromatic light was corrected with a radiometer/photometer (EG&G Electro-Optics 550-1) and a thermopile (Eppley).

Results

1. Structure of Porous Si Layers

Figure 1 shows photoetching currents vs. potential for the formation of porous Si layers on n-Si electrodes in the water-HF-ethanol solution. The saturated photocurrent increases with the cell temperature as well as the illumination intensity. The temperature dependence may suggest that the saturated photocurrent arises from a certain diffusion limited process such as diffusion of HF or dissolved products through fine pores formed. In the present work, the porous Si layers were formed at photocurrents much lower than the saturated photocurrent.

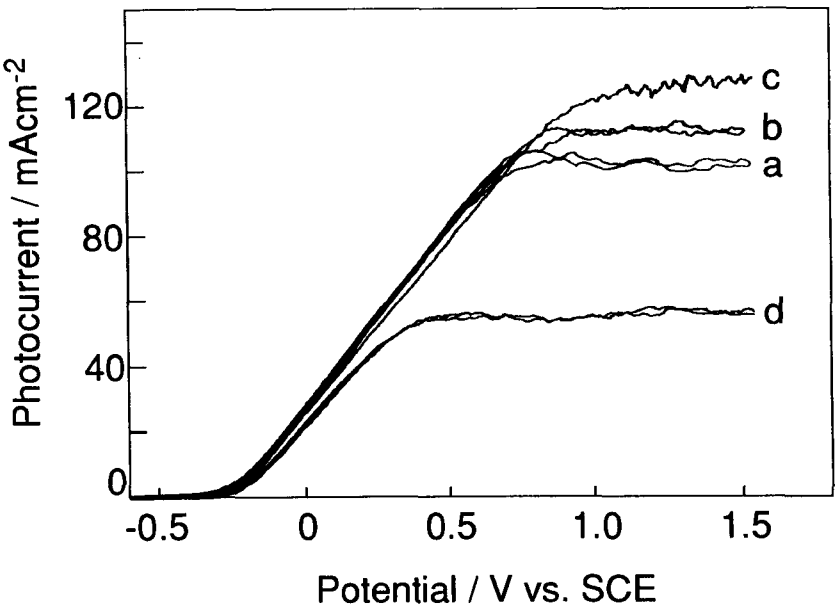

Figure 1. Photoetching currents vs. potential for n-Si in water, 50 % HF and ethanol (21:3:4 in volume). The illumination intensity in $mWcm^{-2}$ and the cell temperature in °C are (a) 180, 30, (b) 180, 40, (c) 180, 50, and (d) 80, 50, respectively.

Figure 2 shows scanning electron micrographs (SEM's) for a porous n-Si electrode prepared by photoetching at 50 $mAcm^{-2}$ under 180 $mWcm^{-2}$ illumination at 50°C for 5 min. The electrode surface has pores and Si pillars of a few micrometers (Fig. 2A and B). The side walls of the Si pillars are covered with a sponge-like layer ca. 0.2-μm thick (white layer with down in Fig. 2B). The sponge-like layer is also present on the top of the Si pillars in an extended form (Fig. 2B). The amount of this layer on the top increased very much, forming a thick continuous layer, when the photoetching was performed at a low temperature, say, 30℃, similar to the reports by Levy-Clement et al [2, 21-23]. The sponge-like layer can be assigned to a nanoporous layer having nanometer-sized pores as explained later.

Figure 2A also shows white parts here and there on the sponge-like layer (part indicated by an arrow). These parts are assigned to Pt-deposited parts as confirmed by EDX analyses. It is to be noted that Pt was vacuum-deposited with the n-Si surface inclined to the direction of the Pt vapor (the incident angle 75°) and thus Pt was deposited mainly on one side of the sponge-like layer.

Figures 3 and 4 show SEM's of n-Si electrodes which were prepared under the same condition as Fig. 2 but, after stop of the photoetching, immersed in the water-HF-ethanol solution in the dark at the same temperature as for the photoetching (50℃) for 40 and 300 s, respectively. The sponge-like layer becomes thinner as the immersion time gets longer. The difference in the size and height of the micrometer-sized Si pillars between Figs. 3 and 4 is merely due to a difference in the inspected part of the electrode. The size and height of the micrometer-sized Si pillars are nearly unchanged by this immersion. The white parts in Fig. 3A and 4A are Pt-deposited parts, similar to Fig. 2A.

A top view

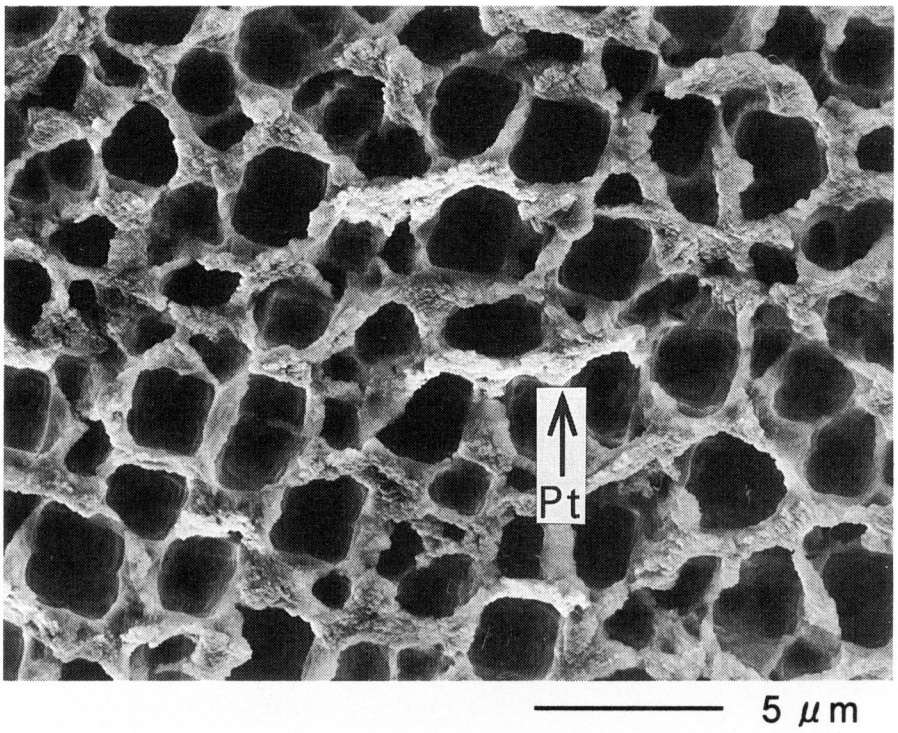

B cross section

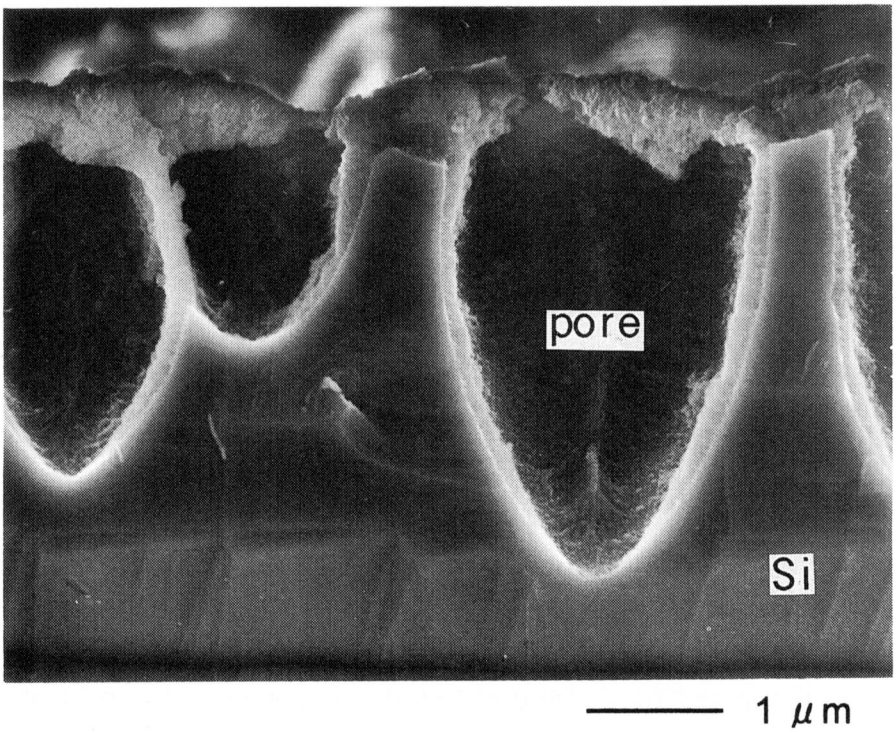

Figure 2. SEM's for a porous n-Si electrode prepared by photoetching at 50 $mAcm^{-2}$ under 180 $mWcm^{-2}$ illumination at 50°C for 5 min and coated with Pt. The arrow shows the Pt-deposited part.

A top view

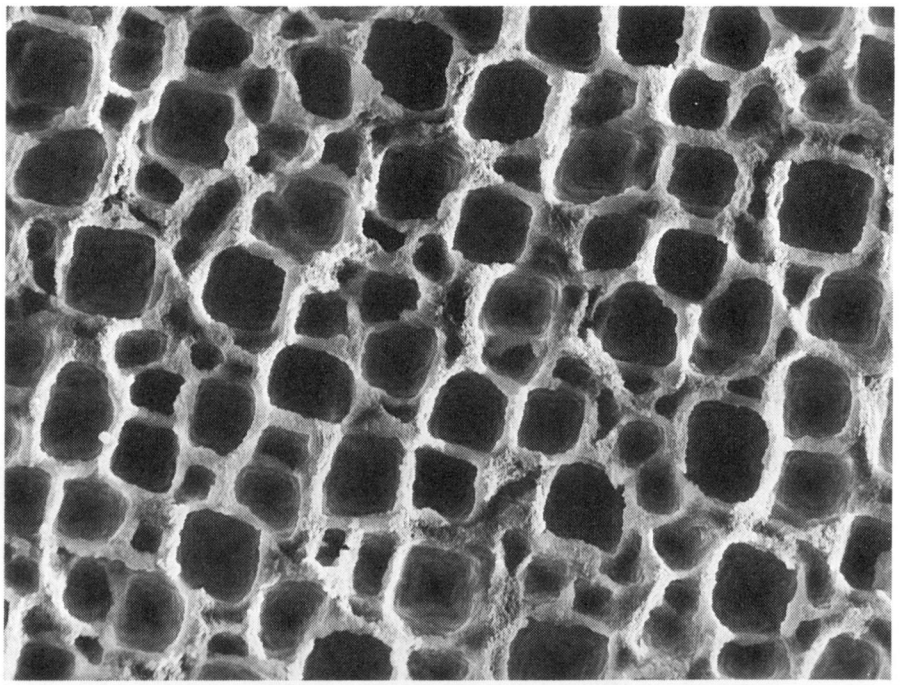

B cross section

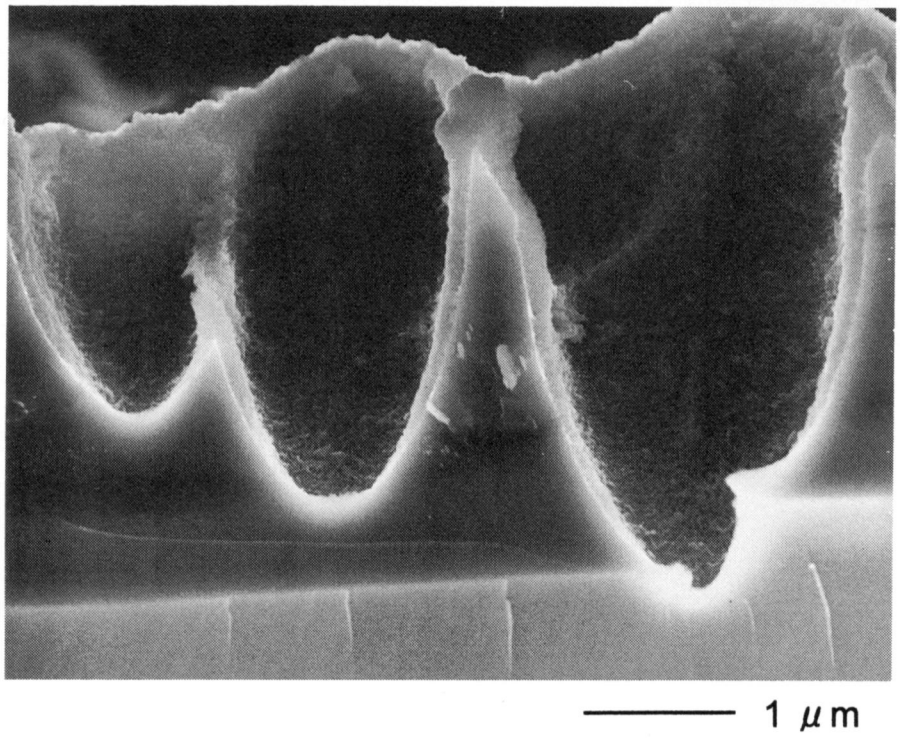

Figure 3. The same as Fig. 2 except that the n-Si electrode was immersed in the water-HF-ethanol solution at 50℃ for 40 s after stop of the photoetching.

A top view

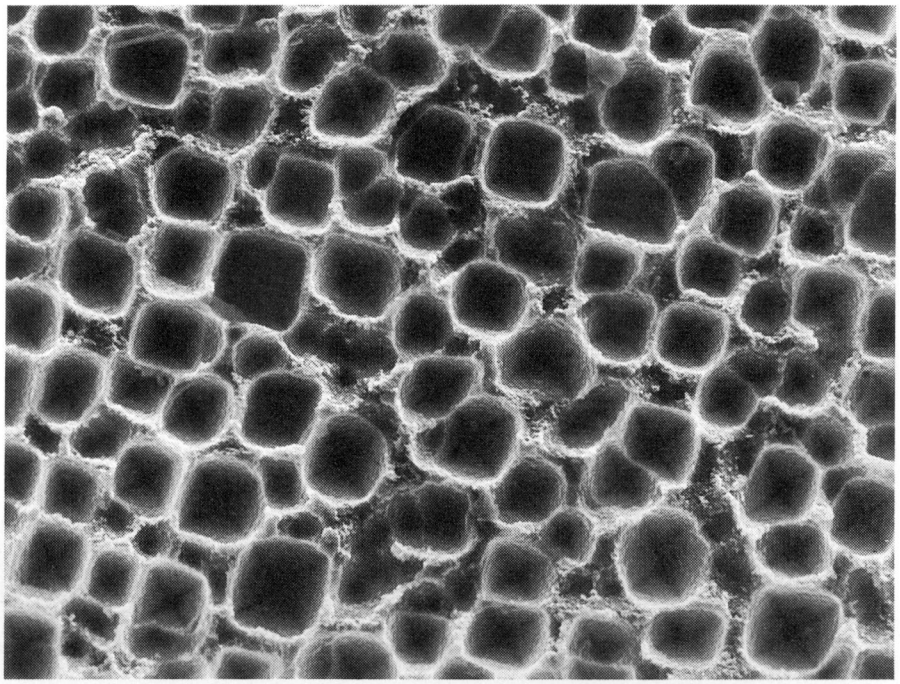

B cross section

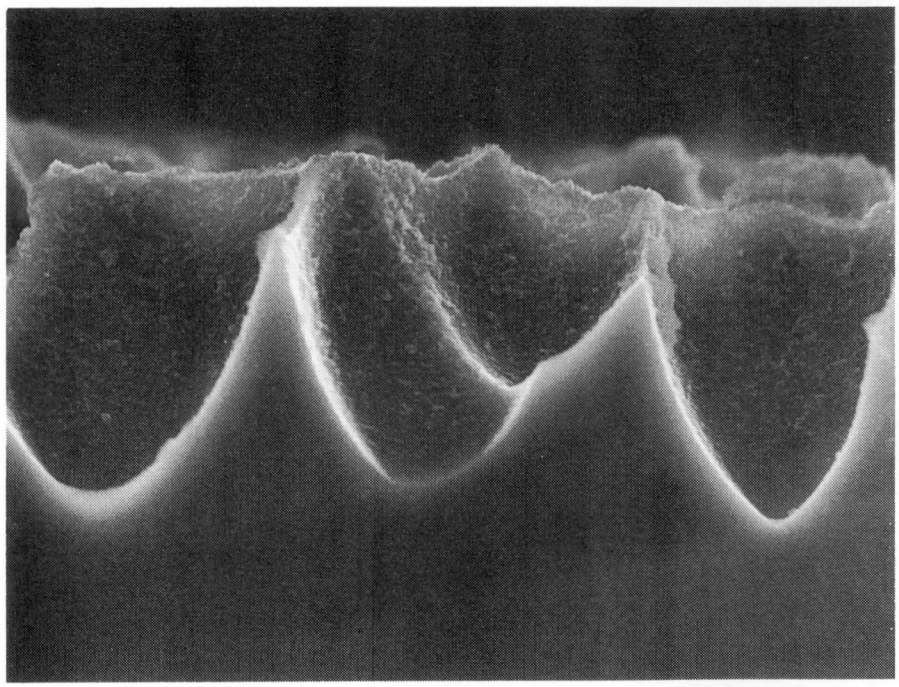

Figure 4. The same as Figs. 2 and 3 except that the n-Si electrode was immersed in the water-HF-ethanol solution at 50℃ for 300 s after stop of the photoetching.

Figure 5A shows a cross-sectional SEM of the sponge-like layer on the side wall of the micrometer-sized Si pillar at a high magnification, and Fig. 5B does the same at a further high magnification. We can see that the layer has nanometer-sized pores and Si nets, like a nest of ants. Similar structure was reported from TEM inspection [24-26]. In white parts of the left side of Figs. 5A and B, Pt is deposited. Pt is present in a relatively extended form.

The n-Si electrodes prepared under the same condition as Fig. 2, hereafter called Fig. 2-type electrodes, showed strong photoluminescence (PL) peaked at 545 nm. The electrodes prepared in the same way as Fig. 3, called Fig. 3-type electrodes, also showed the PL but the intensity was considerably weaker than the Fig. 2-type. The electrodes prepared in the same way as Fig. 4, Fig. 4-type electrodes, showed no PL. This result is in agreement with the above conclusion that the sponge-like layer in the SEM's is the nanoporous Si layer, because the intensity of PL, reported to be emitted from the nanoporous layer [1, 2, 4, 5, 23, 24, 27], decreases with decreasing sponge-like layer. The conclusion is also in harmony with Halimaoui's report that the nanoporous Si layer is dissolved in HF much faster than bulk Si [2, 28]. It is to be noted that the above result indicates that the thickness of the nanoporous layer can be controlled by regulating the immersion time in the water-HF-ethanol solution.

When n-Si was photoetched in a mixture of 50% HF and ethanol (6:1 in volume), its surface had quite a different structure from those of Figs. 2 to 5. The surface had many cracks 2~3 μm wide and about 5 μm deep like the bottom of dried marsh, instead of micrometer-sized pores and sponge-like layers. The surface emitted very strong PL, indicating the formation of a thick nanoporous layer. We hereafter call the electrodes of this type dried-marsh-type electrodes.

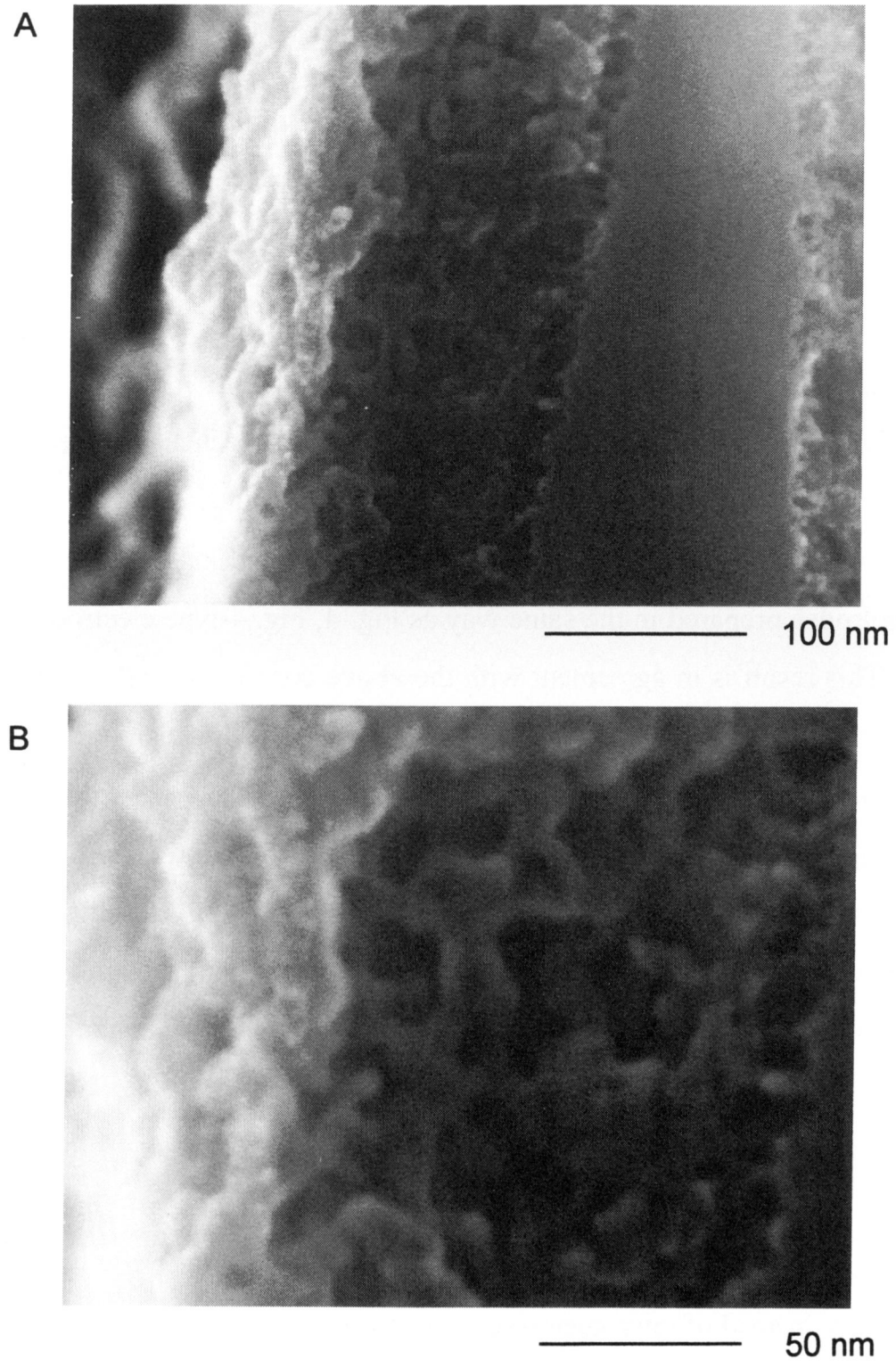

Figure 5. Cross-sectional SEM's of the sponge-like (nanoporous) layer for the Fig 3-type electrode at high magnifications.

2. Solar Cell Characteristics

The photocurrents for the Fig. 2-, Fig. 3- and Fig. 4-type porous n-Si electrodes decayed quickly to zero in 20~30 s without Pt coating. However, they were stabilized to large extents by Pt coating. Figure 6 shows a time course of photocurrent (j) vs. potential (U) for the Fig. 3-type electrode with Pt in 8.6 M HBr/0.05 M Br_2. The photocurrent in a region between 0.0 and -0.3 V vs. counterelectrode was kept constant for 2 h (the electricity flowing during this period of time is 220 Ccm^{-2}) though it afterward decayed to a half in 30 min. The V_{OC} decreased slightly with time during the initial 2 h (Fig. 6). The PL was weakened much after a few cyclic potential scans though the photocurrent itself was not changed at all at this stage.

The photocurrent for the Fig. 2-type electrode was somewhat less stable, a photocurrent of 31 $mAcm^{-2}$ at -0.3 V decaying to 29 $mAcm^{-2}$ in ca. 80 s. This indicates that the presence of a thick sponge-like (nanoporous) layer on the top of the micrometer-sized Si pillars decreases the stability. In fact, the short-circuit photocurrent j_{SC} (the photocurrent at 0.0 V) of 30 $mAcm^{-2}$ for an electrode having a sponge-like layer much thicker than seen in Fig. 2, prepared by photoetching at a low temperature, decayed to 10 $mAcm^{-2}$ in 2 min. On the other hand, the photocurrent for the Fig. 4-type electrode was stable, more stable than that for the Fig. 3-type electrode.

Figure 7 shows the j-U curves for the Fig. 3- and Fig. 4-type electrodes coated with Pt in 8.6 M HBr/0.05 M Br_2 (solid and dot-dashed lines) and 7.6 M HI/0.05 M I_2 (dashed and dotted lines). The redox potentials for the HBr/Br_2 and HI/I_2 are 0.54 and 0.02 V vs. SCE, respectively. The V_{OC}'s for both the electrodes become higher as the redox potential gets higher. Especially, the V_{OC} for the Fig. 3-type electrode in the HBr/Br_2 is much higher than that in the HI/I_2. The difference in j_{SC}

between the HBr/Br_2 and HI/I_2 is due to the difference in the color (light absorption) of the solutions.

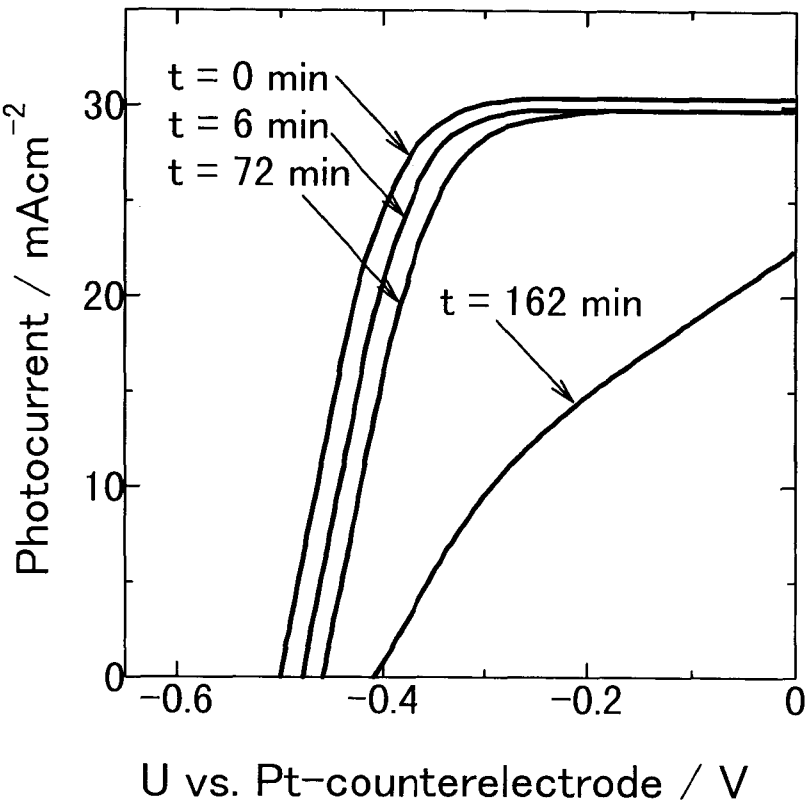

Figure 6. A stability test of the j-U curve for the Fig. 3-type n-Si electrode with 1.8-nm thick Pt in 8.6 M HBr/0.05 M Br_2. The electrode was continuously illuminated at -0.2 V vs. counterelectrode except when the j-U curves were measured intermittently. The t in the figure represents the time passed after the start of illumination.

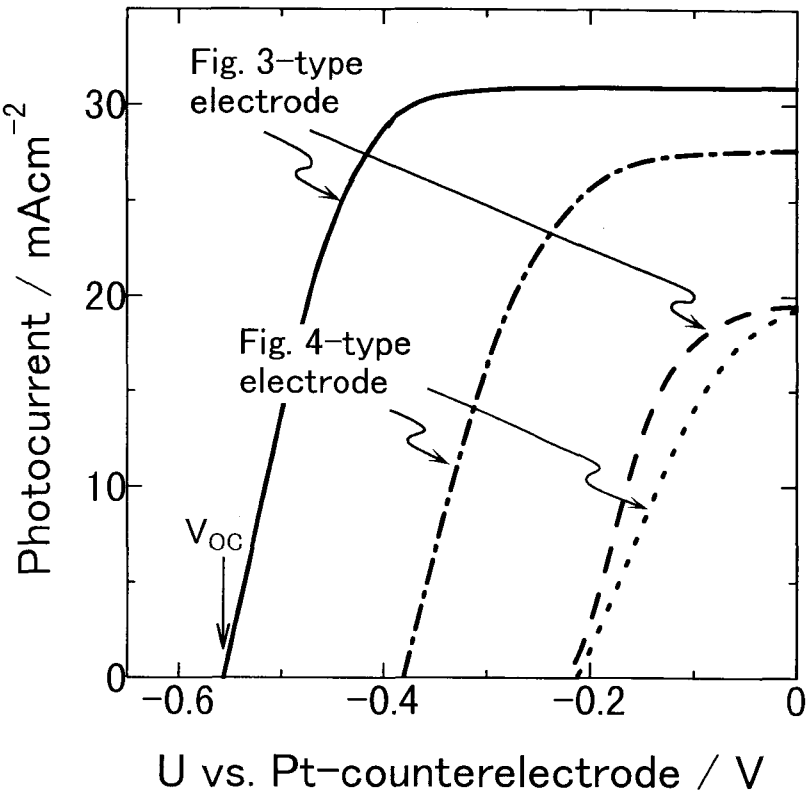

Figure 7. The j-U curves for the Pt-deposited Fig. 3- and Fig. 4-type electrodes in 8.6 M HBr/0.05 M Br_2 (solid and dot-dashed lines) and 7.6 M HI/0.05 M I_2 (dashed and dotted lines) under simulated solar illumination (AM1.5G, 100 mWcm^{-2}).

Table 1 summarizes the solar cell characteristics for various porous n-Si electrodes coated with Pt in 8.6 M HBr/0.05 M Br_2, including those for flat-surface (non-porous) n-Si electrodes. The V_{OC}'s for the Fig. 2- and Fig. 3-type electrodes

range from 0.50 to 0.58 V and are much higher than those for the Fig. 4-type electrodes (0.38～0.42 V), though the latter are still higher than for the flat-surface n-Si electrodes (0.31～0.36 V). The j_{SC}'s for the Fig. 2-, Fig. 3- and Fig. 4-type electrodes are similar to each other, ranging in 25-38 $mAcm^{-2}$, and are much higher than those for the flat n-Si electrodes (22-26 $mAcm^{-2}$). This indicates that the j_{SC}'s are mainly determined by the mat-texture effect of the micrometer-sized pores. The maximum solar energy conversion efficiency of 14.0 % (V_{OC} 0.575 V, j_{SC} 34.7 $mAcm^{-2}$ and the fill factor 0.701) under AM1.5G, 100 $mWcm^{-2}$ illumination was obtained for the Fig. 3-type electrode whose surface structure is just shown in Fig. 3. This efficiency is one of the highest for the n-Si PEC solar cells reported so far [29, 30].

Figure 8 shows the effect of the incident angle (θ) of the Pt vapor during the vacuum-deposition of Pt on the V_{OC} of the Fig. 3-type electrode. The V_{OC} increases with θ, indicating the importance of oblique Pt deposition. The photocurrent action spectrum for the Pt-deposited Fig. 3-type electrode was similar in spectral shape to that for the flat (non-porous) n-Si electrode except that the photocurrent efficiency for the former was higher than that for the latter. The specular reflectance of the porous n-Si electrode at an incident angle of 5° was measured to be nearly zero in wavelengths from 300 to 1300 nm.

The photocurrent for the dried-marsh-type porous n-Si electrode was not stabilized by the Pt coating. It first increased and then decreased, irrespective of the presence or absence of Pt, as reported by Koshida et al. [12] The first few potential scans gave an unusually high V_{OC} of 0.740 to 0.800 V, indicating that the photocurrent is arising from the electrode corrosion.

Table 1. Solar cell characteristics for the Pt-deposited porous and flat (non-porous) n-Si electrodes in 8.6 M HBr/0.05 M Br_2. The lowest and highest values are indicated, with the average and standard deviations in parentheses.

Electrode type	No. of tested samples	V_{OC} (V)	j_{SC} ($mAcm^{-2}$)	F.F.[a)]	ϕ^{S} [b)] (%)
Fig. 2-type[c)]	8	0.506 - 0.580 (0.551 ± 0.022)	24.6 - 36.1 (31.3 ± 3.77)	0.299 - 0.657 (0.477 ± 0.098)	—
Fig. 3-type	30	0.503 - 0.580 (0.550 ± 0.013)	28.4 - 36.1 (31.3 ± 1.30)	0.565 - 0.730 (0.676 ± 0.032)	10.3 - 14.0 (11.7 ± 0.734)
Fig. 4-type	7	0.380 - 0.420 (0.401 ± 0.011)	27.6 - 37.8 (32.4 ± 2.39)	0.530 - 0.726 (0.628 ± 0.045)	5.65 - 9.88 (8.23 ± 1.17)
flat n-Si	6	0.315 - 0.365 (0.337 ± 0.014)	22.3 - 25.8 (24.3 ± 1.30)	0.557 - 0.656 (0.592 ± 0.033)	4.20 - 5.49 (4.84 ± 0.381)

a) fill factor.

b) solar energy conversion efficiency (AM1.5G, 100 $mWcm^{-2}$).

c) All the values are for the first few potential scans because the characteristics degraded with time.

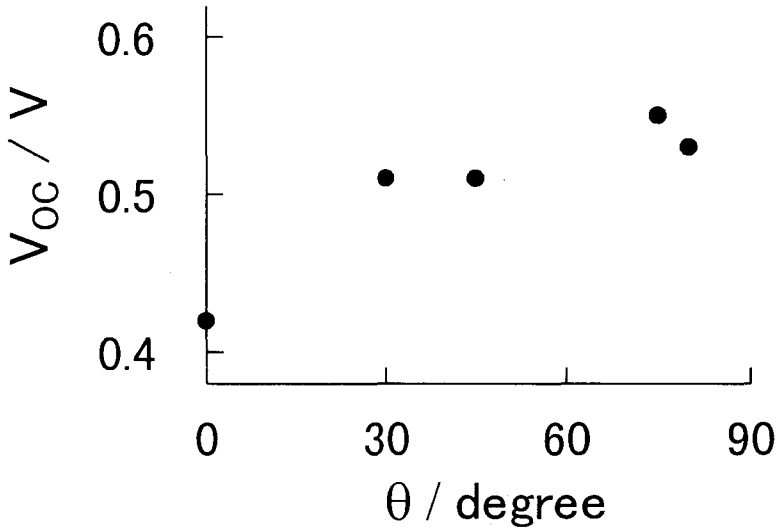

Figure 8. V_{OC} vs. the incident angle (θ) of the Pt vapor during the vacuum deposition of Pt for the Fig. 3-type electrode.

Discussion

From the results described in the preceding section, we can conclude that high V_{OC}'s and stable photocurrents are obtained for the Pt-coated Fig. 3-type porous n-Si electrodes having moderately thick nanoporous layers. The electrodes having too thick nanoporous layers, such as the Fig. 2-type and dried-marsh-type electrodes, generate high V_{OC}'s but are unstable even with Pt. On the other hand, the electrodes having very thin or no nanoporous layers such as the Fig. 4-type electrodes give stable photocurrents but the V_{OC} is low.

It is rather surprising that the Pt-coated Fig. 3-type electrodes generate high V_{OC}'s of 0.50 to 0.58 V, much higher than those for the Pt-coated flat-surface (nonporous) n-Si electrodes (0.31～0.37 V). Also, the photocurrent is fairly stable

(Fig. 5) and furthermore the fill factor is large enough, exceeding 0.7 in some electrodes (Table 1), indicating that the nanoporous layer having the thickness of 0.1 to 0.5 μm has no serious electric resistance to hole transport. Much attention has been paid to the resistivity of the nanoporous layer in relation with the quantum-size effect and surface charges in the literature [25, 26, 31-34], but in the present paper we do not come into the details. They will be reported in a separate paper.

The generation of the high V_{OC}'s for the Pt-coated Fig. 3-type electrodes can be explained as follows. A schematic cross-sectional view of the electrode surface is shown in Fig. 9 on the basis of Fig. 5. Pt is present only on the top of the nanoporous layer in a rather extended form. The electrode is stabilized only with Pt. These facts indicate that photogenerated holes in n-Si bulk come out through the nanoporous layer to Pt and cause oxidation reaction at the Pt surface with the redox couple. The electrolyte solution will be able to penetrate into the nanometer-sized pores and thus the surface of the nanometer-sized Si nets within the nanoporous layer will be covered with thin Si oxide (1.0-1.3 nm thick as estimated from XPS analyses for flat n-Si surface [29]). Such an oxide layer is expected to be formed either electrochemically in highly oxidative 8.6 M HBr/0.05 M Br_2 solution or photoelectrochemically upon illumination. Thus, the major part of the Si surface of the porous n-Si electrode is covered with thin Si-oxide and in contact with the electrolyte, Pt being present sparsely only on the top (Fig. 9). Such a surface structure is quite similar to that for the flat-surface n-Si electrode modified with ultrafine Pt particles reported previously [17, 18]. Hence, almost the same concepts can be applied to the present electrode. According to our previous work [17, 18], the n-Si electrodes with nanometer-sized Pt-dot contacts generate high V_{OC}'s for the following reasons: (1) The barrier height in a redox solution is nearly equal to that for a naked (or thin oxide covered) n-Si electrode, almost free from Fermi

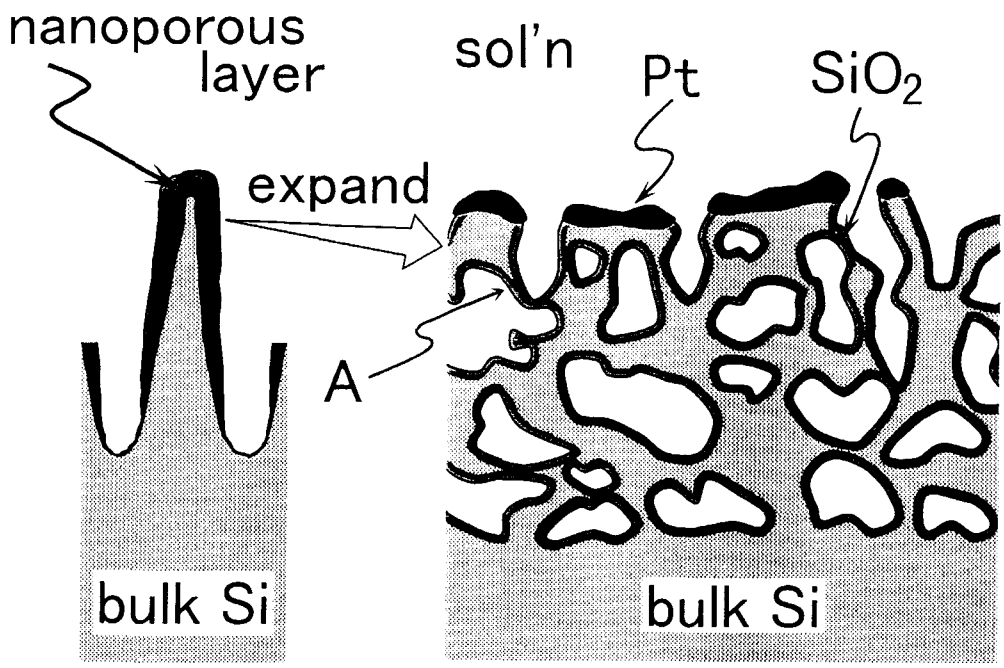

Figure 9. Schematic cross-sectional view of the Pt-coated Fig. 3-type porous n-Si electrode.

level pinning in the n-Si/Pt direct contact areas. Therefore, the barrier height can increase up to the bandgap (the maximum barrier height) in case where the redox potential of the solution is largely positive enough. This is because the modulation of the surface band energies of n-Si by deposited Pt particles (islands) is limited spatially only to a region of nearly the same size as the Pt particles and is negligible in case where they are very small [20]. (2) The major part of the Si surface is covered with Si oxide and passivated for surface carrier recombination. These two reasons decrease the dark saturation current density (j_0) very much and hence increase the V_{OC}. Of these two reasons, the reason (2) holds for the present electrode (Fig. 9), but the reason (1) has to be modified slightly.

For the Pt-coated Fig. 3-type electrode, the bulk n-Si is covered with a thick nanoporous layer (0.1～0.5 μm thick) and Pt is present on the top of it. Thus, we can expect that the barrier height for the electrode is essentially determined by the fine (nanometer-sized) Si nets within the nanoporous layer, not by the Pt-Si contacts. This is because the width of the Schottky-type barrier formed at the n-Si/solution interface ranges from 200 to 500 nm and is much wider than the radius of the fine part of the Si nets (Si wires) (cf. Fig. 5B). In other words, almost no space charge layer is present in the fine part of the Si nets (Si wires) and thus the conduction band energy in this part effectively determines the barrier height of the electrode.

The above argument explains why the barrier height (and hence V_{OC}) for the Fig. 3-type electrodes become high. The argument also explains why the V_{OC} for the electrodes increases with increasing the redox potential (Fig. 7). The higher V_{OC} for the Fig. 3-type electrodes than for the Fig. 4-type (Fig. 7) is explained by taking into account that the Fig. 3-type have moderately thick nanoporous layers whereas the Fig. 4-type have only very thin or no nanoporous layers. For the latter electrodes, Pt may be deposited directly on the micrometer-sized Si pillars (bulk Si) with a large area of Pt-Si direct contacts. This leads to low V_{OC} [17, 18].

As mentioned before, the presence of a too thick nanoporous layer decreases the electrode stability. This is also explained by the above model (Fig. 9). If the radius of the Si nets (Si wires) in the nanoporous layer is nearly equal to or smaller than the thickness of the Si oxide layer formed on the Si surface (1.0-1.3 nm as already mentioned), the Si wires are fully oxidized at that part and become insulating for hole transport (part A in Fig. 9). The amount of such fine Si wires between the Pt and micrometer-sized Si pillars (bulk Si) will increase with increasing thickness of the nanoporous layer.

Figure 8 shows that the V_{OC} decreases with decreasing incident angle (θ) of the Pt vapor during the Pt deposition. This can be attributed to the fact that the nanoporous layer is very thin at the bottom of the micrometer-sized pores as can be seen in Fig. 3B.

The highest V_{OC} obtained for the Pt-deposited porous n-Si electrodes, 0.58 V, is still lower than the V_{OC} for flat-surface n-Si electrodes modified with colloidal Pt particles (0.61-0.63 V) reported previously [20, 35]. Because the latter value is expected for the ideal, minority-carrier controlled solar cells [20, 35], this implies that the majority-carrier dark current (j_{0n}) for the Fig. 3-type electrode is still not low enough. A possible reason for this is that the nanoporous Si layer contains thick Si wires here and there and Pt is deposited on such parts. This decreases the effective barrier height and hence increases the j_{0n}. Another possible reason is that the nanoporous layer has a very large surface area (ca. 200 m^2cm^{-3}) [36] and thus the probability of surface carrier recombination increases in proportion to the surface area.

In conclusion, we have studied the structure of the nanoporous Si layer in connection with the photoetching and post-treatment conditions and shown that the control of the thickness of the nanoporous Si layer is important for improving the solar cell characteristics such as the V_{OC}, the fill factor and stability. We have also shown that the micrometer-sized pore formation is effective for increasing the j_{SC}. We have fabricated the solar cells with a high efficiency of 14.0% and discussed an operation mechanism for porous Si-based efficient and stable solar cells.

The stability problem can be solved by extending the solar cells of the present type to solid-state solar cells [18, 37, 38]. The formation of porous Si layers hardly depends on the crystal face of Si, contrary to the mat-texture etching in strong alkaline solutions, and thus the present method can be applied effectively to

Wacker-type polycrystalline Si wafers and to polycrystalline Si thin films. Further studies along this line may lead to a new approach to high-efficiency and low-cost solar cells.

References

1) L. T. Canham, *Appl. Phys. Lett.*, **57**, 1046 (1990).
2) *Porous Silicon Science and Technology*, Edited by J.-C. Vail and J. Derrien, Springer- Verlag, Berlin, Les Edirions de Physique, Les Ulis (1995).
3) R. L. Smith and S. D. Collins, *J. Appl. Phys.*, **71**, R1 (1992).
4) P. C. Searson, J. M. Macaulay, and S. M. Prokes, *J. Electrochem. Soc.*, **139**, 3373 (1992).
5) K. H. Jung, S. Shih, and D. L. Kwong, *J. Electrochem. Soc.*, **140**, 3046 (1993).
6) A. Prasad, S. Balakrishnan, S. K. Jain, and G. C. Jain, *J. Electrochem. Soc.*, **129**, 596 (1982).
7) Y. S. Tsuo, M. J. Heben, X. Wu, Y. Xiao, C. A. Moore, P. Verlinden, and S. K. Deb, *Mat. Res. Soc. Symp. Proc.*, **283**, 405 (1993).
8) W. Guang-Pu, Z. Yi-Ming, H. Zhao-Jian, L. Yu, F. Jing-wei, and M. Yio-Wu, *Sol. Energy Mater. Sol. Cells*, **35**, 319 (1994).
9) G. Sun, Y. Li, Y. Lu, B. Khan, and G. S. Tompa, *Mat. Res. Soc. Symp. Proc.*, **358**, 593 (1995).
10) P. Menna, G. Di Francia, and V. La Ferrara, *Sol. Energy Mater. Sol. Cells*, **37**, 13 (1995).
11) N. Koshida and K. Echizenya, *J. Electrochem. Soc.*, **138**, 837 (1991).

12) H. Koyama and N. Koshida, *J. Electrochem. Soc.*, **138**, 254 (1991).

13) C. Lévy-Clément, A. Lagoubi, M. Neumann-Spallart, M. Rodot, and R. Tenne, *J. Electrochem. Soc.*, **138**, L69 (1991).

14) C. Lévy-Clément, A. Lagoubi, R. Tenne, and M. Neumann-Spallart, *Electrochim. Acta*, **37**, 877 (1992).

15) D. Mao, K. J. Kim, Y. S. Tsuo, and A. J. Frank, *J. Phys. Chem.*, **99**, 3643 (1995).

16) Y. Nakato, K. Ueda, and H. Tsubomura, *J. Phys. Chem.*, **90**, 5495 (1986).

17) Y. Nakato, K. Ueda, H. Yano, and H. Tsubomura, *J. Phys. Chem.*, **92**, 2316 (1988).

18) Y. Nakato and H. Tsubomura, *Electrochim. Acta*, **37**, 897 (1992).

19) S. Yae, I. Nakanishi, Y. Nakato, N. Toshima, and H. Mori, *J. Electrochem. Soc.*, **141**, 3077 (1994).

20) J. G. Jia, M. Fujitani, S. Yae, and Y. Nakato, *Electrochim. Acta*, **42**, 431 (1996).

21) C. Lévy-Clément, A. Lagoubi, and M. Tomkiewicz, *J. Electrochem. Soc.*, **141**, 958 (1994).

22) A. Albu-Yaron, S. Bastide, J. L. Maurice, and C. Lévy-Clément, *J. Lumin.*, **57**, 67 (1993).

23) E. Galun, R. Tenne, A. Lagoubi, and C. Lévy-Clément, *J. Lumin.*, **57**, 125 (1993).

24) A. Albu-Yaron, S. Bastide, D. Bouchet, N. Brun, C. Colliex, and C. Lévy-Clément, *J. Phys. I France*, **4**, 1181 (1994).

25) M. I. J. Beale, J. D. Benjamin, M. J. Uren, N. G. Chew, and A. G. Cullis, *J. Cryst. Growth*, **73**, 622 (1985).

26) V. Lehmann, F. Hofmann, F. Möller, and U. Grüning, *Thin Solid Films*, **255**, 20 (1995).

27) H. Koyama, M. Araki, Y. Yamamoto, and N. Koshida, *Jpn. J. Appl. Phys.*, **30**, 3606 (1991).

28) A. Halimaoui, *Surf. Sci. Lett.*, **306**, L550 (1994).

29) S. Yae, R. Tsuda, T. Kai, K. Kikuchi, M. Uetsuji, T. Fujii, M. Fujitani, and Y. Nakato, *J. Electrochem. Soc.*, **141**, 3090 (1994).

30) J. F. Gibbons, G. W. Cogan, C. M. Gronet, and N. S. Lewis, *Appl. Phys. Lett.*, **45**, 1095 (1984).

31) A. J. Read, R. J. Needs, K. J. Nash, L. T. Canham, P. D. J. Calcott, and A. Qteish, *Phys. Rev. Lett.*, **69**, 1232 (1992).

32) R. Tsu and D. Babić, *Appl. Phys. Lett.*, **64**, 1806 (1994).

33) R. C. Anderson, R. S. Muller, and C. W. Tobias, *J. Electrochem. Soc.*, **138**, 3406 (1991).

34) A. J. Simons, T. I. Cox, M. J. Uren, and P. D. J. Calcott, *Thin Solid Films*, **255**, 12 (1995).

35) S. Yae, M. Fujitani, I. Nakanishi, M. Uetsuji, R. Tsuda, and Y. Nakato, *Sol. Energy Mater. Sol. Cells*, **43**, 311 (1996).

36) R. Herino, G. Bomchil, K. Brala, C. Bertrand, and J. L. Ginoux, *J. Electrochem. Soc.*, **134**, 1994 (1987).

37) Y. Nakato, S. Nishiura, H. Oshika, and H. Tsubomura, *Jpn. J. Appl. Phys.*, **28**, L261 (1989).

38) Y. Nakato, K. Kai, and K. Kawabe, *Sol. Energy Mater. Sol. Cells*, **37**, 323 (1995).

General Conclusion

In this thesis, detailed studies have been made on the single-crystal n-Si electrodes modified with ultrafine Pt particles, with aims of clarifying quantitative relations between the size and the separation of the Pt particles and the solar cell characteristics and verifying the theoretical prediction. The main results are summarized as follows.

In the first chapter, various kinds of colloidal Pt-particles of 5 to 50 nm in diameter were prepared and used for the modification of n-Si electrodes. By a simple method of dropping a Pt colloid solution prepared by Bredig's method, a conversion efficiency of 14.9 % was obtained for an n-Si electrode with a textured surface. This is the highest for the n-Si PEC solar cells ever reported.

In the second chapter, the LB layers of the Pt-colloid particles (2-6 nm in diameter) were first prepared and used for controlling the Pt-particle density on the n-Si electrodes on a nanometer scale. The Pt-particle density was successfully controlled by this method, and it was revealed that V_{OC} was inversely related to the Pt density.

In the third chapter, quantitative studies were made on relations between the Pt density and the solar cell characteristics for the n-Si electrodes modified with the LB layers of the colloidal Pt particles. The ideal n-Si/solution junction and the (ideal) minority-carrier controlled solar cells were obtained for the n-Si electrodes modified with the Pt particles at a low density and heat-treated at a low temperature.

In the fourth chapter, porous n-Si electrodes were used for the control of the size of Pt on n-Si. The thickness of the nanoporous Si layers could be thinned by immersion in HF, and, by using this phenomenon, the size of Pt on Si was controlled on a nanometer scale. The solar cell of a high efficiency of 14.0 % was

fabricated. A new mechanism for porous Si based high-efficiency solar cells is proposed.

These results clearly show that the solar cells of a new type, equipped with n-Si electrodes modified with ultrafine metal particles, are a very promising approach to high-efficiency and low-cost solar cells. The stability of the PEC solar cells is not enough for practical application, but this problem can be solved if the solid-state solar cells of the same type are developed. The method of the present work can be applied effectively to polycrystalline Si thin films. The results described in this thesis are thus very important as a basis for developing the high-efficiency and low-coat solar cells for large-scale practical uses.

Publication List

1. **Preparation of a Langmuir-Blodgett Layer of Ultrafine Platinum Particles and Its Application to n-Si for Efficient Photoelectrochemical Solar Cells**
   Shinji Yae, Isao Nakanishi, Yoshihiro Nakato, Naoki Toshima, and Hirotaro Mori,
   J. Electrochem. Soc., **141**, 3077 (1994).

2. **Efficient Photoelectrochemical Solar Cells Equipped with an n-Si Electrode Modified with Colloidal Platinum Particles**
   Shinji Yae, Ryo Tsuda, Tomoko Kai, Kazuhiro Kikuchi, Masahiro Uetsuji, Takashi Fujii, Morio Fujitani, and Yoshihiro Nakato,
   J. Electrochem. Soc., **141**, 3090 (1994).

3. **Minority Carrier Controlled PEC Solar Cells, Using n-Si electrodes Modified with LB Layers of Ultrafine Pt Particles**
   Shinji Yae, Morio Fujitani, Isao Nakanishi, Masahiro Uetsuji, Ryo Tsuda, and Yoshihiro Nakato,
   Sol. Energy Mater. Sol. Cells, **43**, 311 (1996).

4. **Improvement in Photovoltage and Stability of Porous n-Si Electrodes Coated with Platinum by Regulation of the Thickness of Nanoporous Layers**
   Kazuyuki Kawakami, Takashi Fujii, Shinji Yae, and Yoshihiro Nakato,
   J. Phys. Chem., submitted for publication.

The following papers which are not included in this thesis have been published by the author et al.

5. **Improvement of Amorphous Silicon Solar Cells by Electrochemical Treatments**
   Michio Matsumura, Yuichi Sakai, Shinji Yae, Yoshihiro Nakato, and Hiroshi Tsubomura,
   J. Appl. Phys., **61**, 1648 (1987).

6. **A New Method of Detecting Pinholes Existing in a-Si:H Films**
Yuichi Sakai, Shinji Yae, Michio Matsumura, Yoshihiro Nakato, and Hiroshi Tsubomura,
Solar Energy Mater., **17**, 89 (1988).

7. アモルファスシリコン電極を用いる湿式太陽電池
八重 真治, 中戸 義禮, 松村 道雄, 坂井 裕一, 坪村 宏,
日本化学会誌, 1152 (1988).

8. **Efficient Photoelectrochemical Reduction of Carbon Dioxide on a p-Type Silicon (p-Si) Electrode Modified with Very Small Copper Particles**
Reiko Hinogami, Tomohiro Mori, Shinji Yae, and Yoshihiro Nakato,
Chem. Lett., 1725 (1994).

9. **New Electrochemical Oscillations in Reduction Reactions on a Platinum Electrode in Hydrogen Peroxide Containing Sulfuric Acid Solutions**
Hayato Hommura, Yoshiharu Mukouyama, Toshihiko Matsuda, Shinji Yae, and Yoshihiro Nakato,
Chem. Lett., 391 (1996).

10. **Synchronous Current Oscillations in Electrochemical Reduction Reactions on Two Platinum Electrodes in Sulfuric Acid Solution Containing Hydrogen Peroxide**
Yoshiharu Mukouyama, Hayato Hommura, Toshihiko Matsuda, Shinji Yae, and Yoshihiro Nakato,
Chem. Lett., 463 (1996).

11. **Oscillatory Behavior in Electrochemical Deposition Reaction of Polycrystalline Silicon Thin Films through Reduction of Silicon Tetrachloride in a Molten Salt Electrolyte**
Toshihiko Matsuda, Shinsuke Nakamura, Ken-ichiro Ide, Kazuyuki Nyudo, Shinji Yae, and Yoshihiro Nakato,
Chem. Lett., 569 (1996).

12. **Hole Diffusion Length and Temperature Dependence of Photovoltages for n-Si Electrodes Modified with LB Layers of Ultrafine Platinum Particles**
Jianguang Jia, Morio Fujitani, Shinji Yae, and Yoshihiro Nakato,
Electrochim. Acta, **42**, 431 (1996).

13. **Photooxidation Reaction of Water on an n-TiO_2 Electrode. Investigation of Previously Proposed New Mechanism by Addition of Alcohols to Electrolyte**
Y. Magari, H. Ochi, S. Yae, and Y. Nakato,
ACS Symposium Series, **656**, *"Solid-Liquid Electrochemical Interfaces"*, Edited by G. Jerkiewicz, M. P. Soriaga, K. Uosaki, and A. Wieckowski, Chapter 21 (1997).

14. **Photoluminescence from a Bulk Defect near the Surface of an n-TiO_2 (Rutile) Electrode in Relation to an Intermediate of Photooxidation Reaction of Water**
Y. Nakato, H. Akanuma, Y. Magari, S. Yae, and J.-I. Shimizu,
J. Phys. Chem., submitted for publication.

15. **Mechanism of Synchronous Oscillations for Electrochemical Reduction Reactions on Platinum Electrodes in a Hydrogen-Peroxide Containing Sulfuric Acid Solution**
T. Matsuda, Y. Mukouyama, H. Hommura, S. Yae, and Y. Nakato,
J. Electrochem. Soc., submitted for publication.

16. **New Current and Potential Oscillations for Reduction Reactions on Platinum Electrodes in Acid Solutions Containing High-Concentration Hydrogen Peroxide**
T. Matsuda, H. Hommura, Y. Mukouyama, S. Yae, and Y. Nakato,
J. Electrochem. Soc., submitted for publication.

17. **Modification of Semiconductor Surface with Ultrafine Metal Particles for Efficient Photoelectrochemical Reduction of Carbon Dioxide**
R. Hinogami, Y. Nakamura, S. Yae, and Y. Nakato,
Appl. Surf. Sci., submitted for publication.

総説

1. 湿式太陽電池と表面処理
八重 真治, 中戸 義禮,
表面技術, **45**, 599 (1994).

2. 光電気化学における表面修飾
八重 真治, 中戸 義禮,
電気化学, **63**, 5 (1995).

Acknowledgments

The author would like to express his sincerest gratitude to Professor Yoshihiro Nakato for his continuous guidance, support and encouragement throughout this work. He would also like to express his sincerest gratitude to Professor Emeritus Hiroshi Tsubomura for his guidance early in this work and continuing encouragement.

The author would like to express his deep thanks to Professor Michio Matsumura, Associate Professors Hikaru Kobayashi and Teruhisa Ohno for their valuable advice and discussions. He would also like to express his gratitude to Professor Naoki Toshima (Department of Applied Chemistry, School of Engineering, The University of Tokyo) for his kind instruction on the alcohol reduction method for Pt-colloid preparation, and to Professor Hirotaro Mori and Dr. Takao Sakata (Research Center for Ultra-High Voltage Electron Microscopy, Osaka University) for performing the TEM measurements. The author wishes to thank Mr. Masato Yamada (Shin-Etsu Handotai Co., Ltd.) for donating single-crystal n-Si wafers. He would like to express his appreciation to all of the Professors and Doctors of this Department for their words of wisdom.

Furthermore, the author is grateful to the graduated and the current students who collaborated with him on this project; Ms. Tomoko Kai, Mr. Ryo Tsuda, Mr. Kazuhiro Kikuchi, Mr. Isao Nakanishi, Mr. Masahiro Uetsuji, Mr. Takashi Fujii, Mr. Morio Fujitani, and Mr. Kazuyuki Kawakami. Special thanks are also expressed to Dr. Yuichi Sakai, Mr. Satoshi Sugahara, Mr. Yuichi Miyoshi, Mr. Susumu Terasaka, Mr. Jianguang Jia, and Mr. Asao Toda. The author would like to express his appreciation to Ms. Noriko Wada for her continuing encouragement and support.

Finally, the author wishes to thank his family.